The Impacts of Pulse Discharge Frequencies on Lithium-ion Cell Degradation Using Electrochemical Impedance Spectroscopy

Ruben de Ruiter
University of Twente, Enschede, The Netherlands
Master Thesis

***Abstract*— Understanding the degradation processes of lithium-ion batteries under varying pulse discharge profiles is crucial for the further development of high-performance lithium-ion batteries. This study explores how pulse discharge profiles impact the degradation of nickel manganese cobalt-based (NMC) lithium-ion cells. Focusing on the electrode-electrolyte interface and lithium-ion diffusion, this research systematically investigates the impact of different pulse discharge frequencies (0, 250, f_{Zmin} 850, and 1450 Hz) on battery degradation. This investigation extends beyond the insights provided by Electrochemical Impedance Spectroscopy (EIS) spectrum and its corresponding fitted equivalent circuit model (ECM), but also describes the underlying electrochemical processes. Key findings indicate that contrary to lessons learned for pulse charging regimes, the f_{Zmin} frequency, corresponding to the cell's minimum impedance, resulted in the most significant degradation. This illustrates the dynamic and complex nature of lithium-ion cells response for pulsating loads and highlights the need for specific discharging optimization research which differs from pulse charging theory.**

I. Introduction

Over the past decade, the world's dependency on battery technology has grown drastically [1]. Due to advancements in the energy storage technology, batteries are used in a wide range of applications, from high-demanding military applications and medical devices to cell phones and children's toys [2]. The broad usage of these batteries in various applications has emphasized the need to extend their safety, increase power and energy density while lowering cost and increase lifetime. Lithium-ion batteries are expensive and resource-intensive to manufacture, and they contain hazardous and precious materials like lithium, cobalt and nickel [3]. Recycling these batteries is a complex and energy-intensive process, while also being environmentally harmful [4]. Not only is it important to extend the lifetime of batteries in the sense of sustainability, the usage of batteries in important applications makes it crucial for batteries to not prematurely fail. In addition, second life of battery modules are of growing interest, especially in the context of world wide energy access, in order to be a partial solution for the vast number of electric vehicle (EV) batteries expected to reach end of life in the near future [5]. In order to extract the most usage out of each precious battery, the research field focusing on the causes of battery degradation has been a topic of research for a considered amount of time. The sheer number of papers surrounding the complicated and multidisciplinary topic of battery degradation makes fully understanding and learning the mechanisms of degradation a long and detailed endeavor. A comprehensive literature review on the current state of degradation research can be found in the appendix.

Applications in the field of telecommunication, sensors, medical equipment but also wind turbines and solar systems with fast-reacting Maximum Power Point Tracking devices (MPPTs) generate fast-changing rates of currents, resulting in charge and discharge profiles that are not constant but pulsating in nature. Another typical pulse-demanding load comes from the growing interest in multilevel inverters (MLIs), particularly in sustainable electrical generation and storage systems [6]. All these applications will draw or provide pulses of current from or to the battery

with modulated and shifting frequencies, currents, and duty cycles [7].

With the rise of all these applications, the question arises: Does these pulsating behavior influence the batteries life span? And if this is the case which degradation process is the most important and dominant factor in a lithium-ion battery when it is placed in combination with a pulsed load or supply in comparison to a continuous one? The research done in the field of pulsating power systems and its induced aging of the lithium-ion cell has shown contradicting results up till this moment in time.

G.W. Ngaleu [8] suggests that high-frequency (up to a few kHz) current pulse discharge has detrimental effects on capacity retention, showing almost a five-fold increase in capacity fade (20.5%) in comparison to continuous dc discharge (5.68%). R. Soares [9] investigated the effect of 21 A, 1 kHz pulsating current profile for 300 cycles on a 28 Ah NMC cell, showing no significant capacity fade, 5.2% dc versus 5.3% for the pulsed cells. Finally, L.R. Chen [10] showed that for sinusoidal current ripples applied to the cell during charging at the cell's lowest impedance point, f_{Zmin} being between 900 and 1200 for the NMC cell used, the lithium-ion cell improved in the charging time 17%, the charging efficiency 1.9%, maximum rising temperature 45.8%, and the capacity retention after 1000 cycles being 3.5% higher. P.T. Chen [11] researched the effect of sinusoidal pulse charging and found a 14.5% higher discharge capacity for the pulsating charged cells in comparison to the Constant Current-Constant Voltage (CC-CV) charged cells after 600 cycles.

This spread in findings surrounding the impact of pulsating current shows the scientific gap and lack of understanding what pulsating harmonic signals do to lithium-ion batteries that are designed to operate in dc domain [12]. What is the reason that for certain frequency range and current profile, the effect of pulsating profiles on cell performance seems to be detrimental, while in others, it seems beneficial.

This research paper worked on closing the scientific gap between the electrochemical degradation effect of the more researched, yet still controversial, pulse charging protocols and its application on discharge profiles. Cells were pulse discharged at 250 Hz, 850 Hz and 1450 Hz and their degradation was tracked and compared to dc discharged cells. It is shown that 850 Hz, around the Nyquist plot zero crossing frequency, the degradation was the higher. This, while at 250 Hz and 1450 Hz the frequency was lower than the reference dc cycled cells. Close EIS analysis showed that parameters indicating cathode degradation were higher for the 850 Hz and dc cycled cells in comparison to the 250 Hz and 1450 Hz pulse discharged cells.

The paper starts off with a chapter on explaining the electrochemical theory on lithium-ion batteries, while in section III this knowledge is applied to come up with a deeper understanding on the effects of pulsating currents on lithium-ion battery operation. Section IV describes the experimental setup and provides an overview how this theory is tested. The experimental data is then provided and analysed in section V and VI. Finally, section VII summarizes the paper.

II. Introduction of electrochemical theory

A lithium-ion battery consists of four main elements, illustrated in figure 1: an anode, a cathode, an electrolyte, and a separator. The anode is referred to as the negative electrode and is most commonly made out of a porous graphite layer which is coated on a copper film that acts as a current collector. The cathode is referred to as the positive electrode and is commonly made out of a lithium transition metal (TM) oxide material which can reversibly intercalate the lithium-ions within its lattice structure [13]. Commonly used cathode materials are Nickel Manganese Cobalt (NMC), Nickel Cobalt Aluminium (NCA), and Lithium Iron Phosphate (LFP), which are coated on an aluminum current collector. The medium in which the ionic movement between the two electrodes can take place is called the electrolyte

and consists of a liquid made out of inorganic compounds. To separate the two electrodes from short-circuiting inside the cell, a separator is placed inside the electrolyte which allows for ionic conductivity but is an electrical insulator [3][14][15].

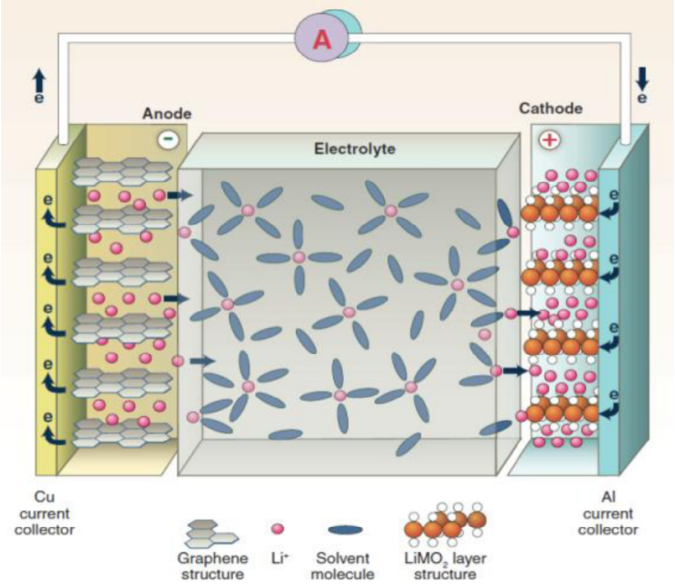

Fig. 1: Diagram illustrating the layout of the primary components that comprise a battery.[16] The separator is placed inside the electrolyte between the anode and the cathode.

When a higher potential than the cell's potential is placed on the cell's terminals, the lithium-ion oxidizes on the positive electrode, diffuses through the positive electrode's lattice of transition metal oxide material, then through the electrolyte, and subsequently reduces at the electrolyte-electrode interface to then travel deeper inside the graphite lattice to eventually intercalate with six carbon atoms to form Li_xC_6 [3]. It is shown that the diffusion of lithium-ions inside the anode containing graphite's lattice and reduction at the electrolyte-electrode interface is slower than the diffusion and oxidation in a positive cobalt oxide lattice like in the positive electrode [17]. When the current applied to the cell is higher than these two anode related limiting factors of diffusion and reduction, a concentration polarization starts to form in the electrolyte near the surface of the electrolyte-electrode interface, which drives the cells' voltage rapidly towards its upper limit [18]. This issue is the reason for the constant voltage part of the charging protocol of CC-CV, in which the cell can charge with constant current until the diffusion reaction in the bulk of the electrode is slowed down to a level at which the applied current is higher than the diffusion speed. By then shifting the charging protocol from constant current to constant voltage, the current drops over time until the electrode is fully utilized [18]. All of this is done in order to keep the cell inside a particular voltage range, to limit the over-potential on the cell which can lead to degradation mechanisms like lithium plating, electrolyte decomposition, excessive SEI formation, and mechanical stresses leading to particle cracking among others [19] [18].

The reason why this explanation of CC-CV protocol is interesting for determining the degradation of pulse discharging a cell, is the fact that pulse charge and discharge protocols have the potential to maintain a higher diffusion reaction rate for longer periods of time during charge and discharge cycles, under certain conditions, like frequency, duty cycle and current amplitude [20]. Electrons can move more freely and faster than that the lithium-ions can intercalate, therefore forming a build up of lithium-ions on the anodes surface when the high current is continuously applied. During the rest period of a pulsating profile, the electrochemical over-potential formed by this build up of lithium-ions on the surface of the electrode- electrolyte interface, can be lowered and redistribute over the surface and eventually stabilize before the next pulse is applied [21]. The application and effects of this approach is still controversial in literature. Most of the research done in this field is conducted on the charging aspect of the theory. Charging protocols can be more easily altered, whereas discharge protocols are harder to change and set because they depend on user behavior. Another reason is that the diffusion of lithium-ions within the bulk of the anode's graphite electrode is typically slower than the diffusion rate in the bulk of the cathode. Therefore, higher yields are expected when this approach is applied to charging as compared to discharging [22][23].

Nevertheless, with the increasing amount of systems consisting of high-frequency switching power electronics, researching the influence of pulsating discharge on the degradation of lithium-ion cells is becoming increasingly relevant over time.

A. Introducing electrochemical impedance spectrum (EIS) as method to measure degradation processes

Looking at the toolbox of characterization techniques available to understand and track degradation, two subsections can be made: *in situ* and *ex situ* techniques. *In situ* measurements consist of techniques that can be utilized during operation, while *ex situ* applications involve removing the sample from the system, and in some cases even disassembling it for analysis [24]. While these *ex situ* techniques can provide valuable insights into the origin and quantity of the actual degradation processes, they require specialized skills and equipment, which are not at the disposal of the author.

In situ measurements, on the other hand, can be done while the system is in use and can be performed in a non-invasive way. These techniques can still provide in-depth information on the specific degradation phenomena present inside the cell. Two widely used methods for distinguishing and tracking degradation in lithium-ion cells are Electrochemical Impedance Spectroscopy (EIS) and Incremental Capacity Analysis (ICA) [25]. While ICA has the benefit of being easy to implement and requiring low computational power, it lacks the precision capabilities required for a more insightful and detailed analysis needed for this research [26].

EIS is a powerful and versatile technique widely used in the analysis of electrochemical systems, including lithium-ion batteries. The technique operates by applying a small alternating voltage or current (AC) signal across a range of frequencies, typically from a few millihertz up to kilohertz or higher, and measures the response of the system. It is particularly useful for investigating the processes that occur at the electrode-electrolyte interface and for diagnosing various aspects of the electrochemical interactions within the cell. This is due to the fact that the response of the cell is correlated to specific electrochemical reactions that operate around that respective frequencies [27]. Because different electrochemical reactions have different operating reaction times, distinctions can be made between them. Tracking these reaction times can provide valuable information on the degradation patterns over time [28].

There are two ways to perform an EIS measurement, potentiostatic and galvanostatic. The difference between the two depends on the impedance system the measurement is conducted on. For high impedance systems, potentiostatic EIS is mostly used, which utilizes a voltage-induced ac signal to produce a current response [27]. Due to current sensing limitations, this method is most suitable for high impedance systems. Galvanostatic EIS, on the other hand, uses a current-induced ac signal to produce a voltage response, which is more applicable to low impedance systems. Because of the lithium-ion cell having low impedance values, galvanostatic EIS is mostly used for measurements on such systems [29].

B. Analysis of EIS measurement using ECM elements

The EIS data can be modelled onto a simplified circuit that models the behaviour of a electrochemical battery system, thereby simulating and tracking electrochemical processes [30]. The model uses electrical elements such as resistors (R), capacitors (C), and inductors (L) to represent its behavior. The goal is to design a simplified circuit model that only highlights the essential processes while keeping the element translation physically meaningful [13]. Figure 2 shows a response of a lithium-ion battery cell for typical EIS measurement, plotted in a Nyquist plot, displaying the equivalent circuit elements for the specific frequency regions. In the plot three different regions can be distinguished. As can be seen in figure 2, these three different sections can be assigned to three frequency domains of the main electrochemical mechanisms inside the cell, described from left to right [31];

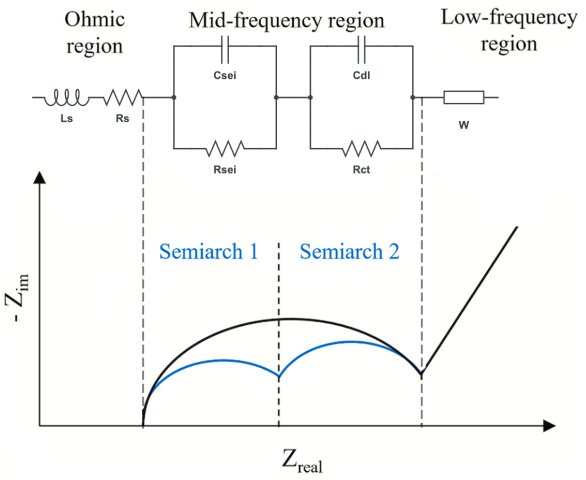

Fig. 2: A redesigned schematic of EIS measurement and the representation of the different frequency regions in a Nyguist plot with a corresponding commonly used equivalent circuit elements [27].

High frequency (above 1 kHz):
The high-frequency part mainly consists of the positive part of the imaginary impedance values. These impedance values are correlated mainly to the inductance of the battery cell windings and wires. When the imaginary axis intercepts the real x-axis, where the inductance behavior becomes substantially less dominant, at the zero-crossing frequency, the ohmic internal resistance of the cell remains, which is the sum of the active material electrical resistance, electrolyte resistance, current collector, and contact resistance. This is also the point in which the inductive impedance is opposite but equal to the capacitive effect of the cell and therefore they cancel each other out [32]. The high-frequency part can therefore be modeled by an inductor and resistor in series, representing the internal ohmic resistance and inductance of the cells' geometry. When the frequency increases further, the real impedance tents to increase again and shifts in the Nyquist plot to the right. This behaviour can be assigned to the skin effect of the current collector at these higher frequencies, in which the concentration of current on the surface increases the ohmic resistance [28]. However, this is beyond the frequency range used in this research, and the influence of skin effect can therefore be neglected [33].

Mid frequency (between 1 kHz and 1 Hz):
In the mid-frequency range of the EIS measurements, two semi-arcs can be detected. These arcs are dominantly caused by the electrochemical behavior of the charge transfer barrier present in the cell. There are two semi-arcs because of the two primarily active charge transfer barriers, which both can be modeled by an RC equivalent circuit element. The two are related to the interface between the electrolyte and electrode surface and the interface between the electrode surface to electrode active bulk material [30].

The first semi-arc is related to the electrolyte-electrode surface interface which are separated from each other by the Solid Electrolyte Interface (SEI) layer[28]. It represents the transport of lithium-ions through the SEI, which is formed due to the decomposition of electrolyte at the electrolyte- electrode interface. The layer's thickness is in the range of nanometers, thickening over time, and is made out of a range of inorganic compounds that form a porous matrix which is ionically conductive[30]. The SEI layer separates the anode active material from the volatile electrolyte, protecting the graphite from being decomposed by the electrolyte solvents[34]. It can be seen as a resistive pathway R_{SEI} for the flow of lithium-ions, because although the SEI is ionic conductive, it still posses a lower conductivity than the electrolyte. Apart from its resistive behavior, the SEI layer also has the ability to store lithium-ions temporarily in and on his surface layer [34]. The SEI can store charges inside its structure because of the pores holes and channels between the inorganic compounds in which lithium-ions can be temporarily and loosely stored inside vacancies in the lattice of the SEI layer or by electrostatic attraction and repelling [33].

The SEI layer can also act as a capacitor because of the separation of charges on the surface. On the electrolyte side, the lithium-ions form a layer close to the interface surface. On the other side is the electrode active material, in which electrons are present that have flowed from the opposite electrode through the external load or charger. The ionic conductivity of the SEI layer is lower than the conductivity of the electrolyte, therefore the SEI layer semi permeable separator.

This opposition of charged ions in the electrolyte and the negative charged electrons in the active material lattice creates a capacitance-like behavior. The schematic separation of charge depicted in figure 3, illustrates the electric over-potential profile across the SEI surface. The capacitance value C_{SEI} is determined by the surface area and the distance between these two charge layers, while also being affected by the over-potential created by the double layer [35][33][36].

The layer of lithium-ions on the surface of the SEI layer creates an electrostatic resistance for other positively charged lithium-ions to flow through the layers into the active electrode lattice combined with the obstructive pathway though the SEI pores and channels can be assigned both as a resistive element. Although the capacitance like impedance does not precisely mimic the behaviour of an ideal capacitor and resistor, this part of the battery cell can be simplified and modeled by an RC element.

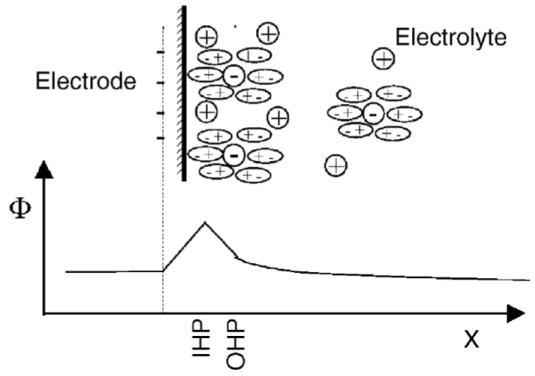

Fig. 3: Grahame model describing the formation of the the double layer capacitor and the potential barrier created [31].

The second semi-arc involves the presence of a double-layer capacitance C_{dl} and charge transfer resistance R_{ct} at the interface between the electrodes surface and bulk of the active electrode material [33] [13]. When lithium-ions diffuse through the porous SEI structure, they reach an SEI-protected bubble containing the active graphite material. This active bulk material also consists of channels and pores that allow lithium-ions to transport throughout the graphite layered structure. During this diffusion, the lithium-ions remain in their ionic form, meaning they have not yet undergone a redox reaction with the active material and are still free to move within the material[37]. The amount of charge that flows through these pores and channels, still in the freely mobile state, is referred to as the double-layer capacitance C_{dl} [33]. These lithium-ions can intercalate into the graphite lattice and undergo a charge transfer reaction with the carbon atoms to form an electrochemical reaction. However, the resistance experienced by the ions as they move through the channels and pores of the electrode during this intercalation process is known as the charge transfer resistance R_{ct}[36][3]. It is found that the R_{ct} places an important role, as it accounts for approximately 60% of the total cell resistance and is related to the kinetics of the electrochemical reaction [13].

The diffusion and transport within the pores and channels of the anodes active material is recognized to be the rate-limiting factor, being the slowest transport process throughout the entire cycle [37][17]. When charging current exceed this diffusion speed, lithium-ions build up on the surface of the anode material, triggering an increasing over-potentials which will initiate lithium plating [36]. Unlike the anode, where the SEI layer is prevalent, the cathode typically exhibits a thinner SEI layer, referred to as Cathode Electrolyte interface (CEI) [38]. The cathode's active material is more directly exposed to the electrolyte, while at the anode the contact is more indirect. The advantage of a more indirect contact is the protection it offers against further degradation. However, this issue is less relevant at the cathode due to its higher potential compared to the anode. In addition, the crystal structure of NMC cathode material is more rigid and uniform, allowing for better ion conductivity in comparison to the more specific pathway restricted transport of ions in the graphite layers. The volume expansion of the anode material can also have an ion transport obstructive effect which can block pores and pathways, which is less prevalent at the rigid NMC structure. This is the reason why the cathode's charge transfer is faster and can respond more quickly to current demands, explaining why battery cells can typically handle faster discharge

rates than charge rates.
To conclude, the RC behavior of the lower mid-frequency part of the EIS measurement can be primarily attributed to the more dominant influence of the anode's R_{ct} and C_{dl} [39][27]. However, it is worth noting that this simplification may instigate that the values of the double layer capacitance and charge transfer resistance are somewhat constant, this is not case. Care needs to be taken doing EIS measurements in order to keep impacting parameters like State Of Charge (SOC) and temperature constant between the different EIS measurements [27].

Low frequency (below 1 Hz):
In the low frequency region of the EIS measurement, a characteristic feature is a straight 45 degrees linear line along the negative imaginary axis as the real impedance increases. This behavior is most commonly associated with the diffusion of lithium-ions within the bulk of the electrode active material lattice, often also referred to as mass transfer and the EIS low frequency tail [35]. This feature is typically modeled in equivalent circuit representations by an element known as the Warburg element. The Warburg element represents a non-intuitive component that cannot be directly correlated with a physical element. This is due to the fact that its phase angle, α, does not align with the conventional phase angles of a capacitor or inductor, but rather falls between these two elements [40]. The impedance of the Warburg element can be expressed as follows:

$$Z_W = \frac{1}{W(j\omega)^{\alpha}} \tag{1}$$

With W being the Warburg element coefficient ($s^{\alpha}\Omega^{-1}$). For standard physical elements like resistors, capacitors, and inductors, this complex impedance equation simplifies to values of α equaling 0, -1, and 1, respectively. In the case of the Warburg element, α is set based on the angle of the low frequency tail relative to the real impedance axis, which is typically at 45 degrees, resulting in an α value of 1/2 and becomes dominant below 1 Hz[41] [42]. Since the interaction of the Warburg element with the system begins to become significant below 1 Hz, this element is neglected due to the fact that is lies outside the pulsating frequency scope used in this research [42] [43].

C. Degradation mechanisms linked to EIS analysis

In the appendix, a detailed review paper can be found that explain and highlights the five primary causes of degradation, namely the growth of the SEI layer, lithium plating, cathode metal dissolution, and particle cracking & fracturing. These processes are all interconnected with three main underlying modes of degradation: loss of lithium inventory, loss of active material, and impedance increase. From the user's perspective, all these degradation modes result in two main noticeable effects: capacity fade and power fade. These effects can only partially be controlled by the use, having only influence on three external factors that impact degradation: temperature, State Of Charge (SOC), and charge/discharge profile. An overview of the interplay between these factors can be seen in figure 4.
Degradation does not follow a singular path towards the end of a cell's life; multiple paths can be identified that lead to its end of use. The interconnected nature of the processes occurring inside the cell makes explaining and predicting the non-linear degradation a complex endeavor. One possible path that can be taken to explain this behavior is the growth of the SEI layer, which leads to increased anode over-potential, thereby opening up the possibility of lithium plating and further SEI growth [44].

Knowing that different sections of the EIS measurement corresponds to different processes, a link need to be made between these processes and degradation in order to distinguish different degradation trend of the different cell groups. Research by T.P. Heins [39], among others [45], stated that the charge transfer resistance, R_{ct}, is an important parameter and an increase of the resistance is the primary response of active material degradation which results in rapid capacity decline. It is stated that a higher R_{ct} will results in a higher over-potential during discharge as well [46]. Another comprehensive research review into the translation of EIS trends to degradation mode concluded that for 78% of the case studies showed that the increase in ohmic region can be translated to Loss of Lithium

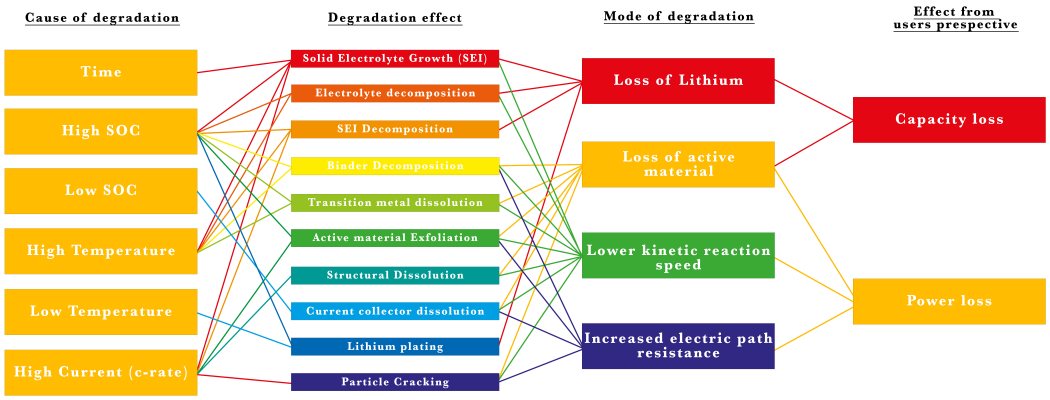

Fig. 4: The complex interaction between the underlying degradation processes and their interplay in contribution to each other *recreated by inspiration from* [3].

Inventory (LLI). 78% of the outcomes explained the first semi-arch increase to be caused by LLI and Loss of anode Active Material (LAM). The second semi cycle was determined to be linked to Loss of cathode Active Material (LAM) for 61% of the studies outcomes [27]. Of the 61% of cases linking LAM to the second semi-arc, 18% addressed this to be caused by particle cracking and 43% to CEI layer formation. Figure 5 shows the outcome of the comprehensive research review investigating a total of 92 paper of which 38 paper included the second semi-arc into their analyses. Of those 38 paper, 15 studies did their experiments on NMC based cathode chemistry. Knowing the link between EIS measurement and proven degradation effects, an detailed analysis can be made to determine the impact of pulse discharge on certain cell degradation, explained in the next section.

III. Optimal Pulsating Discharge Frequency

Referring back to the Nyquist plot, seen in figure 2, the optimal frequency for efficient charge transfer from an electrical engineering perspective is identified at the point of minimum real impedance, this is where the imaginary impedance component equals zero. At this point the capacitive and inductive effect of the cell cancel each other out, become opposite and equal to each other, at this frequency the cells' impedance becomes minimized [47]. This frequency can also be found by looking at the zero point of the angle theta ϑ seen in figure 6. This frequency, denoted as f_{Zmin} [7], has been explored in pulsating charging protocols, yielding mixed results. Some studies report benefits such as improved capacity retention, higher efficiency, and reduced power fade compared to dc charging [48] [49] [50], while others find no significant correlation [9] or even detrimental effects [6][51]. Figure 7 shows the results of pulse charging frequency and their impact on the overall lifetime of the cell at 50% duty cycle [52].

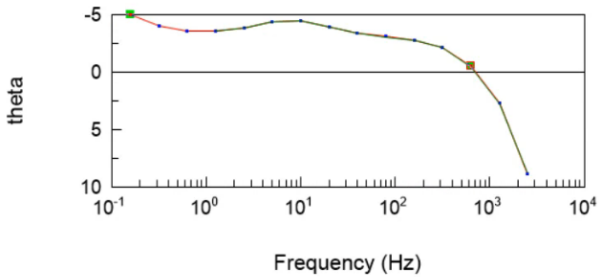

Fig. 6: Angle theta plotted against the applied frequency in an EIS measurement.

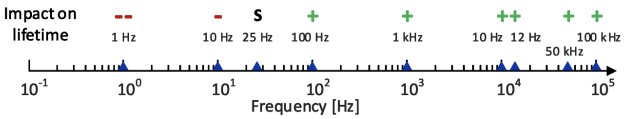

Fig. 7: Results of different studies on the impact of charging frequency on the cycle life of the cell. The red minus sign represents negative impact, green plus sign a positive effect and the black S a negligible non impact. [52]

However, the impact of f_{Zmin} on discharge protocols has gotten less attention in research.

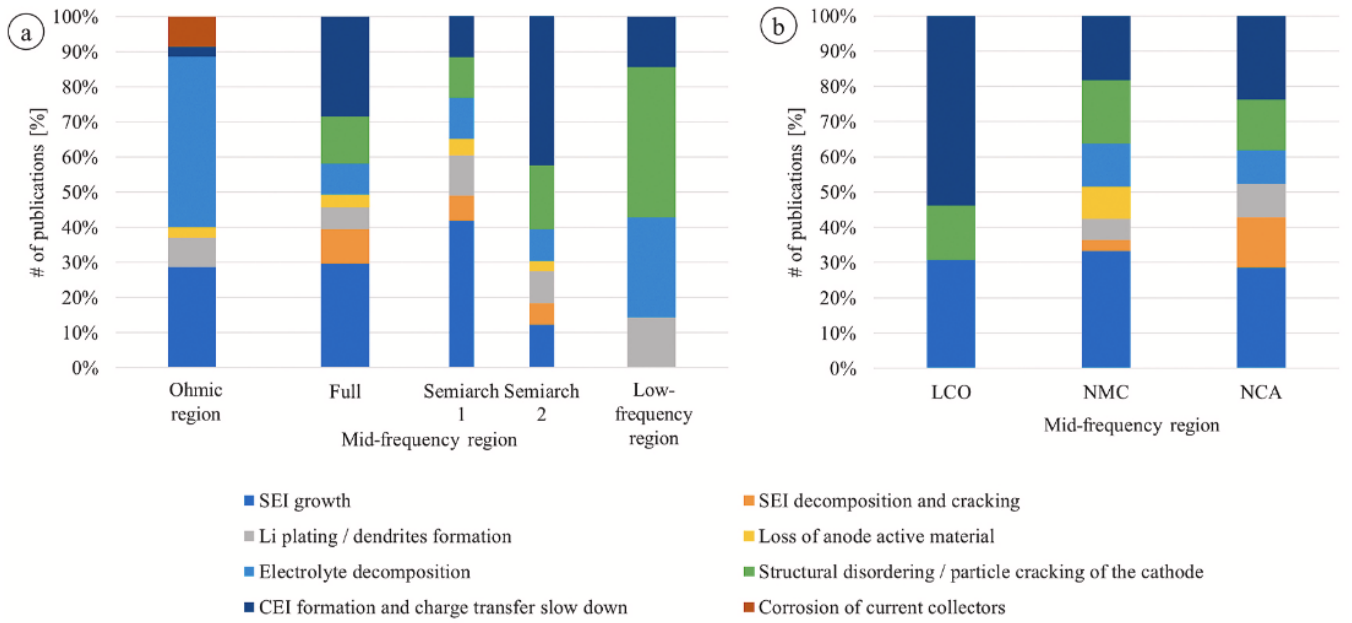

Fig. 5: (a) The graph shows the distribution of reported dominated degradation modes of each frequency region for all chemistry's. (b) Shows the distribution of dominate degradation processes for the three different cathode materials, LCO, NMC and NCA [27].

This paper uses f_{Zmin} as a reference frequency for establishing pulsating discharge parameters.
Looking at this optimal pulse theory from the ECM perspective shows that when a pulsating current is applied to, or drawn from, a lithium-ion cell, the current divides between the charge transfer resistance (R_{ct}) and the double-layer capacitance (C_{dl}), as could be seen in figure 2. The capacitor accumulates charge until its capacity is reached, after which the current flows exclusively through R_{ct}. In other words, the combination of C_{dl} and R_{ct} acts as a low-pass filter for high-frequency components. Research using EIS measurements and ECM has linked the increase in R_{ct} to degradation and inefficiencies, resulting as capacity and power fade [13][45][53]. Therefore, leveraging the buffer effect of C_{dl} to reduce stress on R_{ct} could enhance charging efficiency and mitigate degradation. Several studies support this potentially beneficial effect, demonstrating promising outcomes with pulsating charging protocols [48][49][50][52]. From these findings the intriguing line of reasoning comes to mind if these benefits could also be found when pulsating current profiles were used on the discharge protocol.
However, an opposite reasoning can be made by looking at the amount of current put through the cell at once, the higher pulse current could also increase battery degradation due to correlation between amount of energy flowing through the battery and degradation mechanisms [54]. Also, the pulsating signal is still composed out of a significant dc part, the buffer effect of the C_{dl} only affects the ac current ripples from the pulsating current profile [7]. This might reduce the effectiveness of the rectangular pulsating signal.
Therefore, it can be shown that by only looking at the analysis of the EIS impedance response, the reference optimal pulsating frequency could be found but the analysis can not be directly used to clarify the potential positive results.

In order to understand how these positive results found in charge regimes can be explained, the underlying mechanisms missed by the simplified perspective of the electrical engineering ECM need to be considered. These mechanisms explain the electrochemical characteristics of the double-layer capacitance and their effect on the polarization and conductivity of the lithium intercalation. It highlights the nature of the charge resistance R_{ct}, which is a dynamic parameter together with the double layer capacitance C_{dl}.
Going back, when the current starts to flow in a

pulsating pattern, at the beginning of the pulse, the double-layer capacitor will charge up. Meaning that the lithium-ions are still able to freely move and stored on the surface the lattice of the active material. If the double-layer capacitor reaches saturation, the positive ions will accumulate at the electrodes surface and pores, forming an increased polarisation resistance and conductivity is reduced because of it [47][55] [53]. At dc charging and discharging this increased polarisation resistance will influence the charge transfer, creating an over-potential. Utilizing pulse charging and discharging offers the ability to discharge the concentrated polarisation during the rest period in between pulses, lowering the over-potential and therefore lowering the charge transfer resistance for the next pulse [56][31]. This characteristic of discharging the over-potential has been used and proven to suppress lithium plating during low environmental temperature and high current charging [57][58].

Which makes sense, as explained previously, the accumulation of lithium-ions on the surface of the lattice of the active material leads to an increased resistance. This increased resistance results in an over-potential, which leads to a higher voltage drops across the charge transfer barrier. If this potential difference drops below 0 V versus Li/Li^+, it will trigger lithium plating [59]. In other words, the lithium is moved through the SEI layer faster than it can diffuse and intercalated in the lattice, it will accumulate at the active materials surface, and when the concentration become to high, they start reacting with each other. So the effect of suppressed lithium plating, which will result in lower degradation and higher capacity retention, due to pulsating protocols can hereby be explained [60].

Another way to look at it is given by E. Qu, who states ”*The situation in a porous electrode differs in important ways from that of a simple series RC circuit. The essential difference between a porous electrode and a planar one lies in the distribution of the double layer capacitance coupled in series-parallel ways with the solution resistance. In this case, small but significantly with the resistance of the matrix of the porous material. Thus, for a porous electrode the IR-drop, Ohmic dissipation of energy,* I^2R*, and ion transfer rate are no longer single-valued quantities at a given current, but vary down the pore. The local I, which is determined by local ion and electron transfer rate, diminishes and the cumulative resistance increases owing to a continuous increase of electrolytic resistance down the pore from its orifice.*” [46]
To sum up, the porous structure of an electrode together with the electrode-electrolyte interface forms a dynamic behaviour which can be roughly translated by two RC elements but does not in any form remain constant over time and space. It is highly depended on the current density and profile. Therefore detailed analysis drawn only from electrical ECM perspective do not hold. E. Qu later continuous to elaborate that the surface utilization, so the effective usage of the surface area on the electrodes to mitigate over-potential, is related to the porosity of the electrode and electrode-electrolyte interface, as well as the conductivity of these porous structures. Therefore E. Qu is agreeing with Y.D Lee’s [47] theory on conductivity and saturation.

Another characteristic to track degradation and cell performance, besides capacity retention and EIS measurements, is the temperature of the cell. When considering cell heating effects, four main processes are identified: resistive dissipation, the entropy of cell reactions, side reactions, and the heat of mixing [61]. Among these, resistive dissipation, is the only source of heat generation proven to be dependent on ac frequency [51]. This heat generation power can be roughly estimated as:

$$P = I^2 \cdot Z_{Cell} \tag{2}$$

This observation leads to the compelling hypothesis: cycling a cell at this specific frequency, f_{Zmin}, where the impedance is at its lowest, the heat generation could be minimized. Since lower heat generation is linked to reduced SEI formation and growth, operating at f_{Zmin} could potentially mitigate degradation effects such as capacity and power fade [44].

This effectively means that the extraction of electrical energy from the chemical energy inside

the cell has an optimal efficiency frequency. Consequently, this approach ensures the highest possible energy transfer efficiency by optimizing the electrochemical reaction within the battery [49]. This theory is tested by tracking the cells' temperatures during the experiment to see if this reasoning can be used to validate the hypothesis.

To summarize, looking from the ECM perspective, a case can be made that when the ac impedance is at its lowest, the losses are minimized and lower heat generation will result into the degradation to be minimized. Nevertheless, this only applies for the ac signal component, which is not significant enough to be measurably beneficial to the overall cell performance. Also, the ac signal can be explained to increase the RMS current through the cell, therefore increasing self heating losses and potentially even facilitate faster degradation. However, this perspective sees the resistance of the cell as a constant measurable value, although the resistance encountered by the cell is not at all constant but dynamic in its behaviour, especially during pulsating conditions. By utilizing the optimal charge and discharge protocols, this resistance can be minimized.

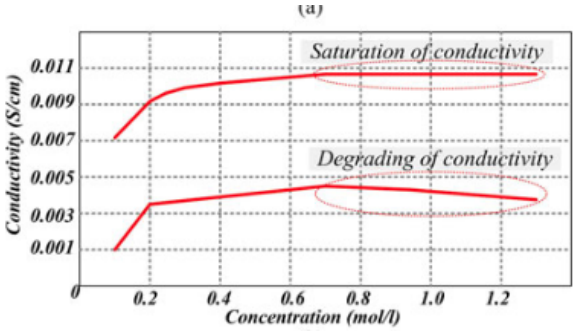

Fig. 8: Describing the relationship between concentration of lithium-ions and the conductivity of on electrodes surface [47][55].

IV. Method and Experimental Setup

A. Experimental setup

In order to validate the effectiveness of these pulsating discharge profiles, experimental research is needed to explore the frequency range for this theory to hold. The experimental procedure was conducted utilizing Samsung INR18650-30QT-6 lithium-ion cells. Each cell has a capacity of 3000 mAh, a nominal voltage of 3.6V, and is capable of sustaining a continuous discharge rate of 15A, as well as a charge rate of 4A. These cells were selected in collaboration with another research project that also focuses on these cells. The project involves energy access, where the cells could be used for small household batteries and mobility applications. Both applications may consist of load profiles made from pulsating behavior. The cells are composed of NMC with mixed NCA parts as the cathode material, while the anode is made out of graphite. Looking at the product range of 18650 cells of Samsung, the 30Q cell is a mid range battery which compromises between the energy density and power density.

12 cells were arranged into four groups of three. Each group underwent cycling at distinct frequencies: dc, pulsating rectangular pulse of 250 Hz, f_{Zmin} 850 Hz, and 1450 Hz, which are chosen to be a equal repetition from the f_{Zmin}. The pulsed current groups had a duty cycle of 50%, with a current amplitude of 6A per cell, while the dc group was continuously discharged at the average pulse current of 3A, equivalent to 1C. This is done in order to keep the average current drawn equal to eliminate the effect of different energy throughput between the cells. The cell setup with the shunt resistors and thermocouples can be seen in figure 9. Although not visible in figure 9, thermal paste is used at each temperature sensor in order to ensure good thermal connection to the cells' surface.

The experimental setup incorporated a Chroma 6314A programmable electronic load, which consists of four individual Chroma 63103A modules. Each module was configured to discharge its corresponding group of cells at the specified frequency. These modules can discharge up to 300 W, with a maximum current of 60A and an operational voltage window up to 80 V. The load is capable of generating internal waveforms to perform dynamic loading with cycles up to 20 kHz and a slew rate of 10 A/µs, making it adequate for this experiment, which demands load profiles of up to 1450 Hz [62]. The current wave forms of the modules are validated by using a Pico TA189 30 A precision current probe and GW

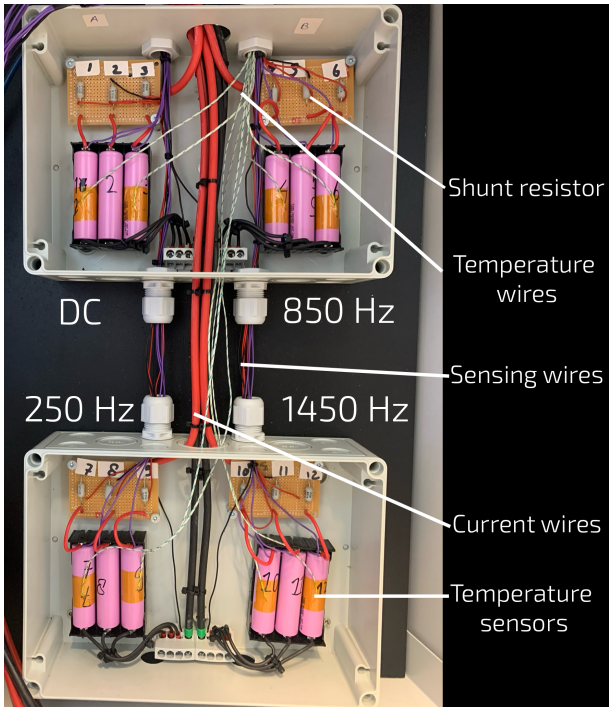

Fig. 9: The layout of the cell distribution in the experimental setup includes the connected current shunt resistors and temperature sensors. On the four labeled breadboards, the shunt resistors are placed in parallel and connected to voltage-sensing wires. The temperature sensors are visible on cells 1, 3, 4, 6, 7, 9, 10, and 12, secured with Kapton tape.

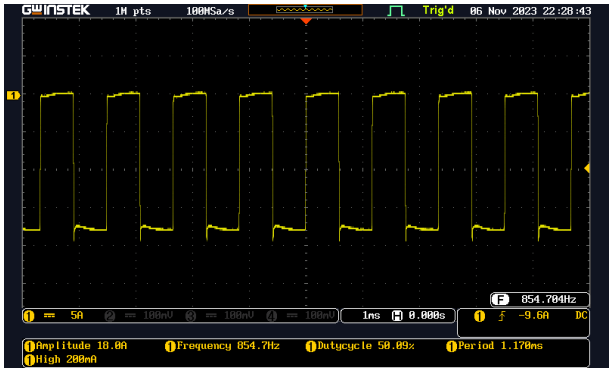

Fig. 10: Current profile of load module two with 850 Hz pulsating waveform.

Instek GDS-1054B oscilloscoop, the waveform of the 850 Hz profile can be seen in figure 10.

The load is connected in parallel to three power supplies by a relay board that is controlled by an Arduino. The relay switch between the load and supplies is necessary to reduce signal noise of the current waveforms deformed by the power supplies parasitic input impedance. The purpose of the three power supplies is to recharge the cells during cycling at a rate of 1C per cell, which will come to a total charge current of 9 A for each cell group. The charging protocol is CC-CV with a cut-off current of 300 mA per cell, 900 mA per cell group. To ensure that each group of cells reaches 100% State of Charge (SOC), it is necessary to isolate the groups during charging. This approach mitigates the impact of varying capacity fade that comes from the experimental discharge profiles. Two digital mono channel EA-PS 3080-20 C supplies are used, capable of delivering up to 80V and 20A with a maximum power rating of 640 W. The third power supplies is a duo channel Keysight E36234A, capable of delivering 80V and 10A and combined maximum power of 400 W for each channel.

Temperature monitoring is conducted using a Pico TC-08 equipped with eight thermocouples, positioned on cells 1, 3, 4, 6, 7, 9, 10, and 12, which can be seen in figure 9 and 11. Due to practical limitations within the setup, only two out of three cells in each group are monitored for temperature. Additionally, to verify the homogeneous current distribution within each cell group, the current of each individual cell is monitored. This is achieved by measuring the voltage drop across a precisely calibrated shunt resistor, which is placed after each cell, and translating this data back into current values with the aid of a Pico Technology ADC-24 voltage data logger. Finally, each group of cells is connected by two sets of wires: voltage sensing wires, connected to both the supplies and load modules, and current feeding wires.

All the various systems are controlled by a custom-made Python script, which not only ensures adequate transition time between the supplies and loads operations and settings but also incorporates safety features to monitor for any instances of overheating, over- and under voltages. The cells are placed within cell holders inside the experimental setup box. This assembly is then housed within a secure, metal battery storage compartment to ensure safety throughout the experiment. A schematic overview of the experimental setup can be seen in figure 11, while the experimental real setup can be seen in figure 12.

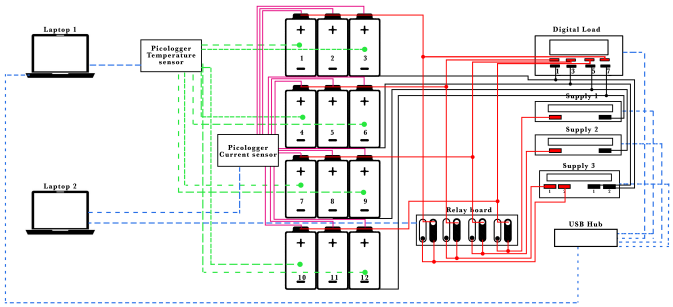

Fig. 11: Schematic diagram of the experimental setup used. The green dotted lines indicate the temperature sensors, the blue dotted lines represent the data USB cables, the red lines depict the positive current wires, the black lines the negative current wires, and the pink wires the current sensor wires. For readability, the voltage sensing wires, which run parallel to the current wires, are omitted in the figure.

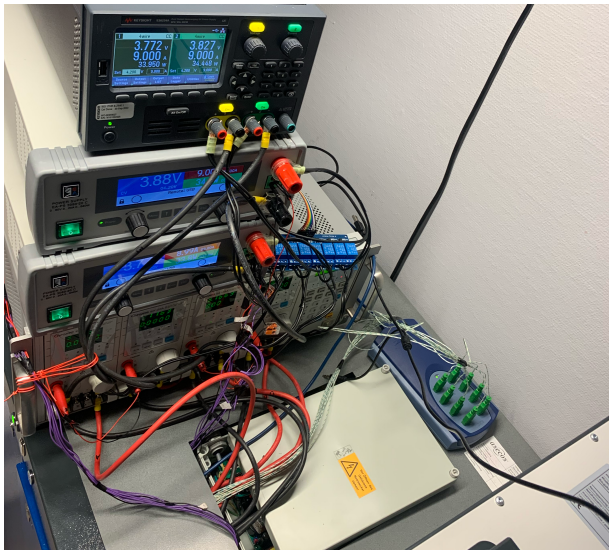

Fig. 12: Experimental setup of equipment used

B. *Cycle process*

At the beginning of the experiment, each cell was labeled, charged to 100% State of Charge (SOC) with a cut-off current of 300 mA, and then allowed to rest for one hour. This rest period lets the cell's diffusion reactions approach a near steady-state equilibrium [8]. Subsequently, the cells were placed in a cell holder connected to the Solartron Analytica XM series for an initial Electrochemical Impedance Spectroscopy (EIS) measurement, conducted in galvanostatic mode over a frequency range of 0.1 Hz to 10 kHz. Afterward, the cells were reinserted into the experimental setup, attached to their respective temperature sensors, and discharged at a continuous dc discharge profile of 1C rate to establish their initial capacity. Once completed, the relay board is engaged to initiate recharging of the cells to 100% SOC until the group current cut-off of 900 mA was reached. This initiated a 5-minute rest period after disconnecting the supplies from the loads by opening the relay board. After this rest period, the load modules were turned on to their specific discharge profiles. Discharge was terminated when cell voltage dipped below 2.7V for more than 3 seconds. Following another 5-minute rest. This process was repeated for 75 cycles, after which the cells were charged to full capacity once more. An hour's rest later, a second EIS measurement was conducted, and the cells were all discharged at a continuous 1C dc load to determine the capacity of each cell. This procedure marked the start of the subsequent sets of 75 cycles.

V. Results and Interpretation

The cells were cycled for 375 cycles, resulting in approximately 85% State of Health (SOH). The following subsections present the results of three measurement domains: capacity fade, cell temperature, and EIS & ECM parameter analysis.

A. *Capacity fade analysis*

The cells were cycled over time, and after each 75 cycles, their capacity retention was measured. Figure 13 illustrates the slope of capacity fade for the four different cell groups. Table 1 displays the capacity fade in comparison to the initial capacity of each cell group. Notably, the capacity fade is highest for the 850 Hz pulsating group, at 13.93%, followed by the dc discharged group at 12.81%. The 250 Hz discharged group performed the best, with a capacity fade of only 12.19%. The 1450 Hz group split the experimental results, showing a capacity fade of 12.53% over 375 cycles. It should be noted that the largest difference in individual cell capacity across all cells was 1.8%.

The standard deviation between the cells' capacities within the groups increased from dc, 850 Hz, 1450 Hz and 250 Hz respectively. The maximal difference between the highest and lowest

cell in the 250 Hz group was 1.47% with respect to the average capacity of the group.

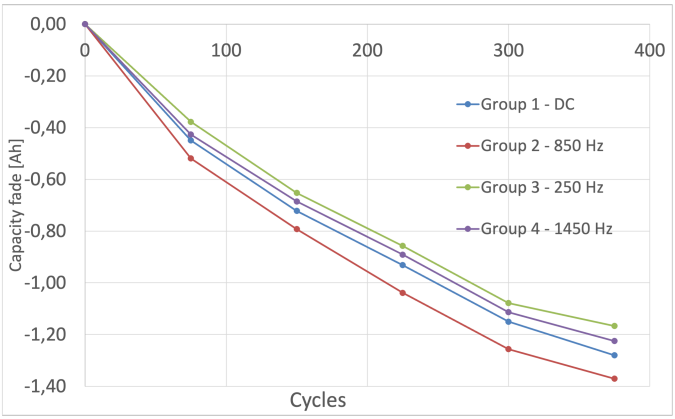

Fig. 13: The slope of the capacity fade of the four groups over the span of 375 cycles

B. Cell temperature analysis

Looking from a temperature point of view, the variation over a single cycle at the 315th cycle is illustrated in figure 14. The graph shows that during the discharging part of the cycle, the cells in the pulsating groups exhibit more rapid heating compared to the group discharged continuously at dc. However, during the charging process, in which all the cell are being charged with the same CC-CV 1C protocol, the continuously dc-discharged group heats up more and eventually reaches a higher temperature compared to the groups of cells discharged with pulsating currents. The maximum temperature is reached by the 250 Hz pulsating group, closely followed by the 850 Hz and 1450 Hz groups. The largest temperature difference within the pulsating groups is 1.72°C, while the peak difference between the highest (250 Hz) and the lowest (dc) at the end of discharge reaches 4.18°C. Looking at the shape of the discharge profile, the cell groups all seem to have the same pattern. This can be explained by the fact that the cells have a higher internal resistance when cell's temperature is relatively low, which is the case in the beginning of the discharge profile. With the SOC lowering during the discharge cycle, the cells' heat generation drops due to an enhanced ionic transfer, which in turn lowers resistance. Consequently, the cell experiences a phase of heat generation which is stable, eventually creating a somewhat temperature plateau. As the SOC further declines, the charge transfer resistance increases due to the cathode becoming increasingly saturated with lithium-ions. Consequently, while the current remains constant, the cells' heat generation will increase again [3].

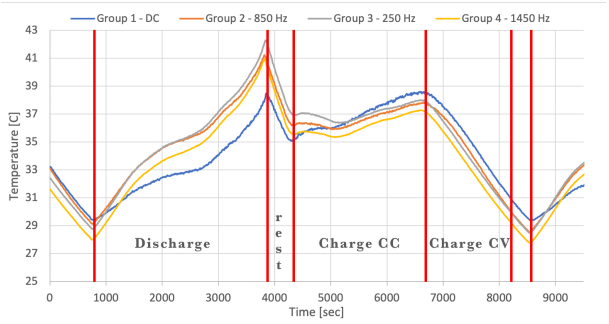

Fig. 14: Temperature profile of the four groups of cells during the 315th cycle. This graph displays the average temperature, calculated from two out of three cells equipped with sensors in each group. Approximately at 800 seconds, the discharge commences, continuing until 3900 seconds, marking the beginning of a 5-minute rest period. Subsequently, around 4200 seconds, the charging cycle initiates. The graph slope clearly shows the temperature decrease when the CV starts and the current drops.

Upon the starting point of the charging half cycle, the dc group temperature slope is notably steeper and reacts faster than the pulsating groups. Heating up almost instantaneously and eventually, nearing the end of the CC charging protocol, the maximum temperature reached by the dc group is 1.37°C higher than the pulsating groups. While the pulsating cells seem to react only slightly when the charging begins, the slope increases briefly, followed by a section in which the temperatures even drops. In contrast, the dc group does not experience this temperature drop and continues to rise, although the slope is less steep. It is crucial to also consider mass temperature inertia, which delays and stretches the temperature rise measured at the surface of the cell in comparison to the temperature inside the cell. This implies that when the pulsating cells had a higher internal temperature, the internal temperature would cool down slower than the surface temperature. Upon the initiation of charging, the heat generation increased, warming up the cell. However, since the internal temperature of the pulsating cells was still higher, leading to lower resistance, the external temperature did not respond as quickly

TABLE 1: This table details the observed total capacity of the four different groups subjected to varying discharge frequencies. The capacity measurements were recorded at specific cycle intervals, denoting the progressive degradation of the cells. The last two columns provide the absolute and relative capacity fade, highlighting the impact of discharge frequency on the battery's cycle life.

Cell group [#]	Frequency (Hz)	Total capacity Cycle 0 [Ah]	Total capacity Cycle 75 [Ah]	Total capacity Cycle 150 [Ah]	Total capacity Cycle 225 [Ah]	Total capacity Cycle 300 [Ah]	Total capacity Cycle 375 [Ah]	Total capacity fade [Ah]	Total capacity fade [%]
1	0	8,985	8,535	8,262	8,053	7,834	7,7039	1,151	14,25%
2	850	9,022	8,503	8,230	7,983	7,766	7,6515	1,257	15,20%
3	250	8,845	8,467	8,191	7,987	7,766	7,6770	1,078	13,20%
4	1450	8,890	8,463	8,205	7,999	7,777	7,6655	1,114	13,78%

at the start of the charging cycle. In contrast, the internal temperature of the DC cell group was lower due to less heating during discharge, resulting in higher resistance and, consequently, greater heat generation at the beginning of the charge cycle.

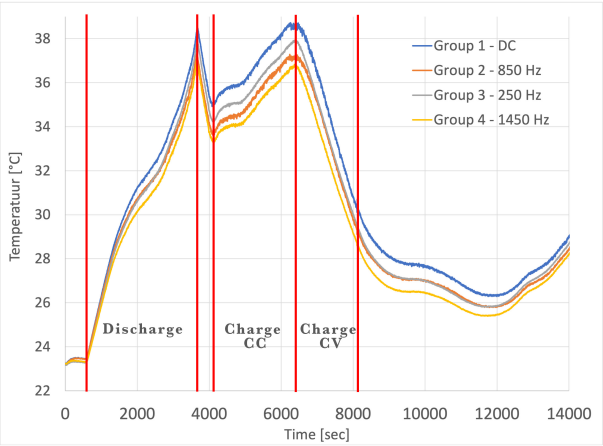

Fig. 15: Temperature profile of the four groups of cells during a collective dc retention measurement cycle. This graph displays the average temperature, calculated from two out of three cells equipped with sensors in each group. At approximately 500 seconds the discharge start, until 3700 seconds, which initiates the 5 minute rest period, after which at approximately 4000 the charging cycle starts. Noticeably, the dc cycled cells remain higher in temperature during the collective dc charging and dc discharging cycle.

During the capacity retention test, conducted at the end of each 75 cycle period, it was observed that the dc cell group registered the highest temperatures during both charging and discharging phases. This occurred when all cells underwent a collective dc cycle, as depicted in figure 15. During this cycle the relative SOC and charging current where identical, having only a slighter higher charging time difference between the cells which was within one minute of each other. The fact that the dc group 1 experienced a higher temperature slope during the charging part of the normal cycling period, as well as during both the charging and discharging phases of the dc capacity measurement cycle, disproves the notion that the observations are insignificant due to potential measurement noise.

It is worth noting that the difference between charging and discharging temperatures seem to be counter intuitive with the previous proposed hypothesis of lowering polarisation gradients during pulse discharging. In order to validate if any resistance is indeed higher at the dc cells, an analysis of the EIS in combination with the ECM is considered in the next analyse section.

C. Electrochemical Impedance Spectroscopy analysis

After every 75 cycles, an EIS measurement was conducted on each cell. Figure 17 depicts the average impedance of each group at cycle 0 and at the end of cycle 375. As observed in figure 17, the most significant impedance growth is attributed to the 850 Hz pulsating discharge group 1, followed by the dc discharged group 2. Groups 3 and 4, operating at 250 Hz and 1450 Hz, respectively, exhibit a similar but lower impedance rise over time. It can also be observed from figure 17 that the impedance rise is primarily present in the second semi-arc in the mid-frequency range.
The cells were placed in a cell holder during cycling and transferred to another cell holder for EIS measurements. Because the cells needed to be swapped for measurement, the physical connection of the Solartron EIS equipment to

the cells' terminals was not optimal. Efforts were made to improve connectivity while maintaining repeatability. Nevertheless, due to this experimental design, the data points of the ohmic resistance shifted by a maximum of 14.4% between measurements, approximately. Nickel plated tabs were spot welded on the new cells to see the impact of this resistance deviation and showed an approximately 5 mΩ difference with the cell holder measurements. However, the shape and other element values, apart from R_1, remained consistent between measurements. Therefore, the impact of the shift in R_1 is not considered in the analysis due to the limited precision in the measurement setup.

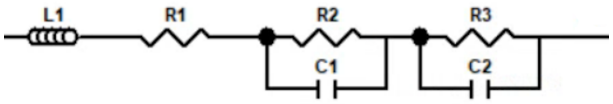

Fig. 16: Equivalent circuit model used in the experiment to fit the EIS measurement on using Z-view software.

The EIS measurement was curve-fitted by Z-view software to match the equivalent circuit model shown in figure 16. The values of the parameters for each group at cycle 0 and 375 are shown in table 2. It is shown that the double-layer capacitance, particularly of the second RC element, increased drastically for all groups. The double-layer capacitance of both the 250 Hz and 1450 Hz pulsating discharge groups exhibited particularly substantial growth. The ohmic region and first semi-cycle demonstrated a more uniform degradation pattern across all groups, with the DC and 850 Hz groups exhibiting a slightly larger increase in the first semi-arc. A noteworthy observation is the increase of charge transfer resistance 31% and 34% for the 250 Hz and 1450 Hz pulsating groups respectively, while the charge transfer resistance of the dc and 850 Hz groups increased significantly, approximately doubling, 89% and 130% respectively.

The interpretation from both the EIS analysis and the capacity fade analysis are consistent, indicating that the group with the highest increase in the EIS measured semi-arc corresponds to the group with the highest capacity fade. The findings of T.P. Heins [39], do align with the observed R_{ct} values in relation to capacity fade, indicating that a greater increase in R_{ct} corresponds to a more present capacity fade. While the 250 Hz and 1450 Hz groups exhibited the least degradation and the smallest growth in the EIS second semi-arc.

VI. Discussion

To formulate an explanation for this observed behavior, the logical starting point is to revisit the degradation pathways of a cell, as illustrated in figure 4 and explained in detail in the appendix. The fundamental causes of cell degradation are typically simplified in an ECM to match EIS responses. Degradation modes include loss of lithium inventory (LLI), loss of active material (LAM), reduced kinetic reaction speed, and increased electrical path resistance, which are illustrated in figure 4. These are influenced by several factors, including SEI formation, electrolyte decomposition, and transition metal dissolution.

Findings showed that during collective DC charge and discharge capacity retention measurements, the temperature differences between the groups was small. However, they remained consistent even after re-calibrating the cell temperature sensors, suggesting a non-negligible effect. The higher temperature observed in the dc-cycled group 1 during charging and discharging indicated greater heat generating losses compared to the 850 Hz group. However, EIS measurements indicated higher impedance and ECM parameter values for the 850 Hz group 2 than the dc group 1, presenting a contradiction.

Hence, the hypothesis is that the 850 Hz pulsating group 2 may have experienced a different degradation pathway compared to the dc group 1. Considering the degradation processes, the question comes up what might cause a relatively higher capacity fade in the 850 Hz group 2 without significantly affecting ohmic impedance, which would otherwise lead to higher heat generation during the dc capacity retention test.

The review analyzing EIS measurements and their link with degradation mechanisms [52], as

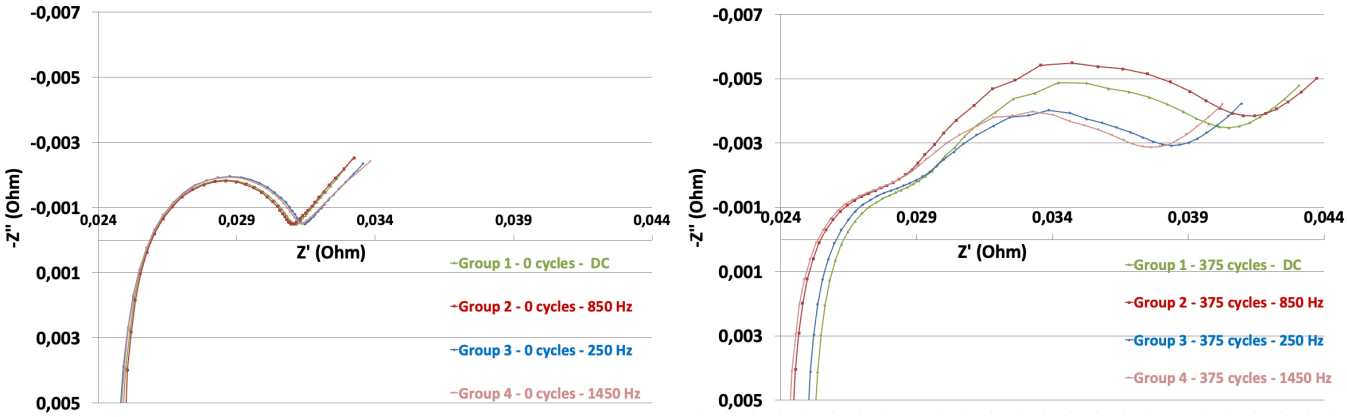

Fig. 17: The change in EIS measurement graph between cycle 0 and cycle 375.

TABLE 2: Equivalent circuit model parameters at 0 cycles and after 375 cycles.

Cell parameters	Cycle 0 dc	Cycle 375 dc	Cycle 0 850 Hz	Cycle 375 850 Hz	Cycle 0 250 Hz	Cycle 375 250 Hz	Cycle 0 1450 Hz	Cycle 375 1450 Hz
L1 [µL]	0,301	0,322	0,302	0,318	0,303	0,328	0,298	0,328
R1 [mΩ]	24,688	20,673	26,103	19,67	24,959	18,001	26,078	17,08
R2 [mΩ]	2,636	1,129	2,681	1,228	2,693	1,033	2,627	1,024
C1 [F]	0,098	0,308	0,102	0,306	0,093	0,394	0,096	0,398
R3 [mΩ]	2,829	5,347	2,759	6,348	2,991	3,928	2,949	3,960
C2 [F]	0,472	8,104	0,497	7,872	0,450	9,046	0,452	8,700

seen in figure 5, suggests that an increase in the second semi-arc could result from significant cathode-related degradation. The pulse discharge at 850 Hz could have enhanced particle cracking and CEI formation. Resonant vibrations oscillating at this frequency can cause small cracks in the NMC particles, which may grow over time, leading to the fragmentation of the cathode material and resulting in a loss of active cathode material. On the other hand, the higher temperature observed in the dc cycled cell during the 1C discharge and charge cycles suggests increased internal resistance, possibly due to the growth of the SEI layer on the anode. SEI growth is the most commonly observed degradation phenomenon in normally operating lithium-ion cells [44].

The cathode related degradation in dc cell group 1, indicated by also a significant increase in the second semi-arc, can be attributed together with the higher temperature of these cells during collective dc cycling to be caused by transition metal dissolution from the cathode active material into the electrolyte. These transition metals are drawn to the lower potential of the anode where they react with the SEI layer, forming a thicker or more resistive SEI layer [3]. This higher resistive SEI layer leads to more heat generation during collective dc cycling in comparison to the pulsating groups.

These distinct degradation pathways might be a plausible explanation for the counter-intuitive observations seen in the results, where the highest second semi-arc and capacity decay did not correspond to the group with the highest temperature during identical dc cycling. This explanation of difference in degradation pathways mentioned could be validated by doing ex-situ destructive research on the cells. Using Scanning electron microscopy (SEM) to look at the surface roughness and X-ray photoelectron spectroscopy (XPS) could be used to determine the structure and composition of the SEI layer compounds on both the electrodes and in the electrolyte.

VII. Conclusion

This study presents a comprehensive analysis of experimental research on the degradation effects of pulse discharging on lithium-ion cells. Through experimentation and detailed Electrochemical Impedance Spectroscopy (EIS) analysis, it is shown that different pulse discharge frequencies notably impact cell degradation. Interestingly, cells pulsed at approximately 850 Hz, corresponding to the frequency of minimum impedance f_{Zmin}, exhibited the most significant degradation which was predominately observed in the second semi-arc of the Nyquist plot. These EIS results suggest that cathode related degradation is a primary contributor to this notable decay. The degradation pattern of the 850 Hz cell group 2 may be more closely related to CEI formation and mechanical stress, leading to capacity fade and more pronounced EIS changes. In contrast, the degradation pattern in the dc-cycled cell group 1 suggests cathode related degradation as well as anode-related degradation, particularly SEI layer growth, resulting in higher operational temperatures. The different cycling methods impose various stressors on the cell components, leading to these distinct degradation pathways.
These finding contradicts the notion of optimal efficiency found during pulse charging at f_{Zmin}. The theory of this found charging regime is that pulsating current drawn from the cell reduces over-potential at the electrode-electrolyte interface. This lower over-potential results in higher uniformity of current distribution and conductivity, which then suppresses degradation processes such as electrolyte decomposition, SEI formation and transition metal dissolution ultimately leading to higher capacity retention. While some studies have reported the detrimental effects of pulse discharges and charges, others have found neutral or positive outcomes. The capacity fade observed in the 850 Hz group aligns with the findings of G.W. Ngaleu [8], who noted a significant increase in capacity fade with high-frequency pulsating charge and discharges. However, the relatively stable performance of the 250 Hz and 1450 Hz groups found in this research suggest another optimal pulsating frequency then the one found by the conventional pulsating charging research.

This difference in findings highlights the unique and complex behavior of lithium-ion cells under different pulsating conditions and suggests that a one-size-fits-all approach may not be appropriate for optimizing both charging and discharging protocols. Further research is needed to reveal the underlying causes of this behavior and to optimize pulse discharge protocols for enhanced battery longevity and performance. *Ex situ* experiments, such as Scanning Electron Microscopy (SEM) and X-ray Photoelectron Spectroscopy (XPS), could offer much needed insights into the degradation patterns and validate the hypothesis presented in this paper. Additionally, future research focusing on the effects of sinusoidal pulse waveforms in comparison to the rectangular pulse used in this research could provide valuable information for optimizing discharge profiles and give insights into their specific degradation mechanisms. In addition, research in determining the optimal waveform design could investigate pulse waveforms that consist out of different duty cycles or a negative pulse discharge followed by a much briefer positive pulse charge which could enhance the reduction of over-potential even further. This study, therefore, gives reason to further study the optimal regime for discharging the cell, although shown to be of less importance in the past in comparison to charging protocols, this study shows that improvements can definitely be made in the development of more durable and reliable battery systems, by utilizing optimized discharge regime of the lithium-ion battery operation.

VIII. Acknowledgements

The author gratefully acknowledge the help of Deepak Pratap Singh and Prof.Dr.Ir. Mark Huijben in helping understand certain chemical aspects of battery design. Furthermore, gratitude is due to lab technician Roelof Grootjans for technical support.

References

[1] Eleanor Drabik and Vasileios Rizos. "Prospects for electric vehicle batteries in a circular economy". In: (July 2018).

[2] Michel Armand et al. "Lithium-ion batteries – Current state of the art and anticipated developments". In: *Journal of Power Sources* 479 (2020), p. 228708. ISSN: 0378-7753. DOI: https://doi.org/10.1016/j.jpowsour.2020.228708. URL: https://www.sciencedirect.com/science/article/pii/S0378775320310120.

[3] Jacqueline S. Edge et al. "Lithium ion battery degradation: what you need to know". In: *Phys. Chem. Chem. Phys.* 23 (14 2021), pp. 8200–8221. DOI: 10.1039/D1CP00359C. URL: http://dx.doi.org/10.1039/D1CP00359C.

[4] Zachary J. Baum et al. "Lithium-Ion Battery RecyclingOverview of Techniques and Trends". In: *ACS Energy Letters* 7.2 (2022), pp. 712–719. DOI: 10.1021/acsenergylett.1c02602. eprint: https://doi.org/10.1021/acsenergylett.1c02602. URL: https://doi.org/10.1021/acsenergylett.1c02602.

[5] Ali Almarzooqi, Ashot Mnatsakanyan, and Endika Muruaga. "Management of Used Lithium Ion Batteries of EV in Dubai". In: *2019 IEEE International Smart Cities Conference (ISC2)*. 2019, pp. 514–517. DOI: 10.1109/ISC246665.2019.9071665.

[6] Guy Williams Ngaleu et al. "Influence of Switching on the Aging of High Power Lithium-Ion Cells". In: *Batteries* 8.4 (2022). ISSN: 2313-0105. DOI: 10.3390/batteries8040033. URL: https://www.mdpi.com/2313-0105/8/4/33.

[7] Wiljan Vermeer et al. "A Critical Review on The Effects of Pulse Charging of Li-ion Batteries". In: Apr. 2021, pp. 217–224. DOI: 10.1109/PEMC48073.2021.9432555.

[8] Derek Wong et al. "Impact of high rate discharge on the aging of lithium nickel cobalt aluminum oxide batteries". In: *Journal of Power Sources* 280 (2015), pp. 363–372. ISSN: 0378-7753. DOI: https://doi.org/10.1016/j.jpowsour.2015.01.110. URL: https://www.sciencedirect.com/science/article/pii/S0378775315001263.

[9] Rudi Soares et al. "An Experimental Setup with Alternating Current Capability for Evaluating Large Lithium-Ion Battery Cells". In: *Batteries* 4 (Aug. 2018), p. 38. DOI: 10.3390/batteries4030038.

[10] Liang-Rui Chen et al. "Sinusoidal-Ripple-Current Charging Strategy and Optimal Charging Frequency Study for Li-Ion Batteries". In: *IEEE Transactions on Industrial Electronics* 60.1 (2013), pp. 88–97. DOI: 10.1109/TIE.2012.2186106.

[11] Po-Tuan Chen et al. "Reviving Aged Lithium-Ion Batteries and Prolonging their Cycle Life by Sinusoidal Waveform Charging Strategy". In: *Batteries & Supercaps* 2.8 (2019), pp. 673–677. DOI: https://doi.org/10.1002/batt.201900022. eprint: https://chemistry-europe.onlinelibrary.wiley.com/doi/pdf/10.1002/batt.201900022. URL: https://chemistry-europe.onlinelibrary.wiley.com/doi/abs/10.1002/batt.201900022.

[12] Woojin Choi and Dae-Wook Kim. "Analysis of the Output Ripple of the DC-DC Boost Charger for Li-Ion Batteries". In: *Journal of Power Electronics* 14.1 (Jan. 2014), pp. 135–142.

[13] Choi Woosung, Choi Jae-Young, and Yoon Won-Sub. "Modeling and Applications of Electrochemical Impedance Spectroscopy (EIS) for Lithium-ion Batteries". In: *J. Electrochem. Sci. Technol* (2020). DOI: 10.33961/jecst.2019.00528.

[14] B. Purushothaman and U. Landau. “Rapid Charging of Lithium-Ion Batteries Using Pulsed Currents”. In: *Journal of The Electrochemical Society* 153 (Mar. 2006), A533–A542. DOI: 10.1149/1.2161580.

[15] Joshua P. Pender et al. “Electrode Degradation in Lithium-Ion Batteries”. In: *ACS Nano* 14.2 (2020). PMID: 31895532, pp. 1243–1295. DOI: 10.1021/acsnano.9b04365. eprint: https://doi.org/10.1021/acsnano.9b04365. URL: https://doi.org/10.1021/acsnano.9b04365.

[16] Kang Xu. “Nonaqueous Liquid Electrolytes for Lithium-Based Rechargeable Batteries”. In: *Chemical Reviews* 104.10 (2004). PMID: 15669157, pp. 4303–4418. DOI: 10.1021/cr030203g. eprint: https://doi.org/10.1021/cr030203g. URL: https://doi.org/10.1021/cr030203g.

[17] A. Skundin et al. “The lithium intercalation into graphite from electrolyte and from solid lithium”. In: *Journal of Solid State Electrochemistry* 8 (Dec. 2003), pp. 11–14. DOI: 10.1007/s10008-003-0413-9.

[18] Jun Li et al. “The effects of pulse charging on cycling characteristics of commercial lithium-ion batteries”. In: *Journal of Power Sources* 102.1 (2001), pp. 302–309. ISSN: 0378-7753. DOI: https://doi.org/10.1016/S0378-7753(01)00820-5. URL: https://www.sciencedirect.com/science/article/pii/S0378775301008205.

[19] Mohamed Abdel Monem et al. “Lithium-ion batteries: Evaluation study of different charging methodologies based on aging process”. English. In: *Applied Energy* 152 (Mar. 2015), pp. 143–155. ISSN: 0306-2619. DOI: 10.1016/j.apenergy.2015.02.064.

[20] Chuang-Yaw Lin and Shi-Chern Yen. “The Application of Pulse Charge for Secondary Lithium Battery”. In: *ECS Transactions* 11 (May 2008). DOI: 10.1149/1.2938907.

[21] Huazhen Fang, Christopher Depcik, and Vadim Lvovich. “Optimal pulse-modulated Lithium-ion battery charging: Algorithms and simulation”. In: *Journal of Energy Storage* 15 (2018), pp. 359–367. ISSN: 2352-152X. DOI: https://doi.org/10.1016/j.est.2017.11.007. URL: https://www.sciencedirect.com/science/article/pii/S2352152X17303006.

[22] Jakob Asenbauer et al. “The success story of graphite as a lithium-ion anode material – fundamentals, remaining challenges, and recent developments including silicon (oxide) composites”. In: *Sustainable Energy Fuels* 4 (11 2020), pp. 5387–5416. DOI: 10.1039/D0SE00175A. URL: http://dx.doi.org/10.1039/D0SE00175A.

[23] Jong Park et al. “Investigation of Lithium Ion Diffusion of Graphite Anode by the Galvanostatic Intermittent Titration Technique”. In: *Materials* 14 (Aug. 2021), p. 4683. DOI: 10.3390/ma14164683.

[24] Liu Tongchao et al. “In situ quantification of interphasial chemistry in Li-ion battery”. In: *Nature Nanotechnology* 14 (Jan. 2019). DOI: 10.1038/s41565-018-0284-y.

[25] Carlos Pastor-Fernández et al. “A Comparison between Electrochemical Impedance Spectroscopy and Incremental Capacity-Differential Voltage as Li-ion Diagnostic Techniques to Identify and Quantify the Effects of Degradation Modes within Battery Management Systems”. In: *Journal of Power Sources* 360 (Aug. 2017), pp. 301–318. DOI: 10.1016/j.jpowsour.2017.03.042.

[26] Daniel-Ioan Stroe and Erik Schaltz. “Lithium-Ion Battery State-of-Health Estimation Using the Incremental

Capacity Analysis Technique". In: *IEEE Transactions on Industry Applications* PP (Nov. 2019), pp. 1–1. DOI: 10.1109/TIA.2019.2955396.

[27] Pietro Iurilli, Claudio Brivio, and Vanessa Wood. "On the use of electrochemical impedance spectroscopy to characterize and model the aging phenomena of lithium-ion batteries: a critical review". In: *Journal of Power Sources* 505 (Sept. 2021), p. 229860. DOI: 10.1016/j.jpowsour.2021.229860.

[28] Alexandru Savca. *Application of Electrochemical Impedance Spectroscopy (EIS) on Module Level Li-ion Batteries for Echelon Utilization*. July 2022. URL: http://essay.utwente.nl/92423/.

[29] Daniel-Ioan Stroe et al. "Diagnosis of Lithium-Ion Batteries State-of-Health based on Electrochemical Impedance Spectroscopy Technique". In: (Sept. 2014). DOI: 10.1109/ECCE.2014.6954027.

[30] James Macdonald. "Three to six ambiguities in immittance spectroscopy data fitting". In: *Journal of physics. Condensed matter : an Institute of Physics journal* 24 (May 2012), p. 175004. DOI: 10.1088/0953-8984/24/17/175004.

[31] Andreas Jossen. "Fundamentals of battery dynamics". In: *Journal of Power Sources* 154.2 (2006). Selected papers from the Ninth Ulm Electrochemical Days, pp. 530–538. ISSN: 0378-7753. DOI: https://doi.org/10.1016/j.jpowsour.2005.10.041. URL: https://www.sciencedirect.com/science/article/pii/S0378775305014321.

[32] Wladislaw Waag, Christian Fleischer, and Dirk Uwe Sauer. "Critical review of the methods for monitoring of lithium-ion batteries in electric and hybrid vehicles". In: *Journal of Power Sources* (2014). ISSN: 0378-7753. DOI: https://doi.org/10.1016/j.jpowsour.2014.02.064.

[33] J.R. Macdonald et al. *Impedance Spectroscopy: Theory, Experiment, and Applications, Third Edition*. Jan. 2018.

[34] Cai Shen et al. "Direct Visualization of Solid Electrolyte Interphase on Li4Ti5O12 by in-situ AFM". In: *RSC Adv.* 6 (Aug. 2016). DOI: 10.1039/C6RA16208H.

[35] S.M.M. Alavi, C.R. Birkl, and D.A. Howey. "Time-domain fitting of battery electrochemical impedance models". In: *Journal of Power Sources* 288 (2015), pp. 345–352. ISSN: 0378-7753. DOI: https://doi.org/10.1016/j.jpowsour.2015.04.099. URL: https://www.sciencedirect.com/science/article/pii/S0378775315007569.

[36] Guoxing Li. "Regulating Mass Transport Behavior for High-Performance Lithium Metal Batteries and Fast-Charging Lithium-Ion Batteries". In: *Advanced Energy Materials* 11 (Jan. 2021). DOI: 10.1002/aenm.202002891.

[37] Yongxiu Chen et al. "Revealing the rate-limiting electrode of lithium batteries at high rates and mass loadings". In: *Chemical Engineering Journal* 450 (2022), p. 138275. ISSN: 1385-8947. DOI: https://doi.org/10.1016/j.cej.2022.138275. URL: https://www.sciencedirect.com/science/article/pii/S1385894722037585.

[38] Qingyong Zhang et al. "In situ TEM visualization of LiF nanosheet formation on the cathode-electrolyte interphase (CEI) in liquid-electrolyte lithium-ion batteries". In: *Matter* 5.4 (2022), pp. 1235–1250. ISSN: 2590-2385. DOI: https://doi.org/10.1016/j.matt.2022.01.015. URL: https://www.sciencedirect.com/science/article/pii/S2590238522000157.

[39] Tom Patrick Heins et al. “On the Interpretation of Impedance Spectra of Large-Format Lithium-Ion Batteries and Its Application in Aging Studies”. In: *Energy Technology* 8.2 (2020), p. 1900279. DOI: https://doi.org/10.1002/ente.201900279. eprint: https://onlinelibrary.wiley.com/doi/pdf/10.1002/ente.201900279. URL: https://onlinelibrary.wiley.com/doi/abs/10.1002/ente.201900279.

[40] Claudio Brivio et al. “A Physically-Based Electrical Model for Lithium-Ion Cells”. In: *IEEE Transactions on Energy Conversion* 34.2 (2019), pp. 594–603. DOI: 10.1109/TEC.2018.2869272.

[41] Jun Huang et al. “Graphical analysis of electrochemical impedance spectroscopy data in Bode and Nyquist representations”. In: *Journal of Power Sources* 309 (2016), pp. 82–98. ISSN: 0378-7753. DOI: https://doi.org/10.1016/j.jpowsour.2016.01.073. URL: https://www.sciencedirect.com/science/article/pii/S0378775316300738.

[42] Deyang Qu. “The ac impedance studies for porous MnO2 cathode by means of modified transmission line model”. In: *Journal of Power Sources* 102.1 (2001), pp. 270–276. ISSN: 0378-7753. DOI: https://doi.org/10.1016/S0378-7753(01)00810-2. URL: https://www.sciencedirect.com/science/article/pii/S0378775301008102.

[43] F Croce et al. “An electrochemical impedance spectroscopic study of the transport properties of LiNi0.75Co0.25O2”. In: *Electrochemistry Communications* 1.12 (1999), pp. 605–608. ISSN: 1388-2481. DOI: https://doi.org/10.1016/S1388-2481(99)00123-X. URL: https://www.sciencedirect.com/science/article/pii/S138824819900123X.

[44] J. Vetter et al. “Ageing mechanisms in lithium-ion batteries”. In: *Journal of Power Sources* 147.1 (2005), pp. 269–281. ISSN: 0378-7753. DOI: https://doi.org/10.1016/j.jpowsour.2005.01.006. URL: https://www.sciencedirect.com/science/article/pii/S0378775305000832.

[45] Nina Meddings et al. “Application of electrochemical impedance spectroscopy to commercial Li-ion cells: A review”. In: *Journal of Power Sources* 480 (2020), p. 228742. ISSN: 0378-7753. DOI: https://doi.org/10.1016/j.jpowsour.2020.228742. URL: https://www.sciencedirect.com/science/article/pii/S0378775320310466.

[46] Deyang Qu. “The ac impedance studies for porous MnO2 cathode by means of modified transmission line model”. In: *Journal of Power Sources* 102.1 (2001), pp. 270–276. ISSN: 0378-7753. DOI: https://doi.org/10.1016/S0378-7753(01)00810-2. URL: https://www.sciencedirect.com/science/article/pii/S0378775301008102.

[47] Yong-Duk Lee and Sung-Yeul Park. “Electrochemical State-Based Sinusoidal Ripple Current Charging Control”. In: *Power Electronics, IEEE Transactions on* 30 (Aug. 2015), pp. 4232–4243. DOI: 10.1109/TPEL.2014.2354013.

[48] Rashmi Prasad, Chandra S. Namuduri, and Phillip J. Kollmeyer. “Onboard unidirectional automotive G2V battery charger using sine charging and its effect on li-ion batteries”. In: *2015 IEEE Energy Conversion Congress and Exposition (ECCE)* (2015), pp. 6299–6305. URL: https://api.semanticscholar.org/CorpusID:30216539.

[49] Liang-Rui Chen et al. “Sinusoidal-Ripple-Current Charging Strategy and Optimal Charging Frequency Study for Li-Ion Batteries”. In: *IEEE*

Transactions on Industrial Electronics 60.1 (2013), pp. 88–97. DOI: 10.1109/TIE.2012.2186106.

[50] Fabien Lacressonniere, B. Cassoret, and J.-F Brudny. "Influence of a charging current with a sinusoidal perturbation on the performance of a lead-acid battery". In: *Electric Power Applications, IEE Proceedings* - 152 (Oct. 2005), pp. 1365–1370. DOI: 10.1049/ip-epa:20050008.

[51] Kotub Uddin et al. "The impact of high-frequency-high-current perturbations on film formation at the negative electrode-electrolyte interface". In: *Electrochimica Acta* 233 (2017), pp. 1–12. ISSN: 0013-4686. DOI: https://doi.org/10.1016/j.electacta.2017.03.020. URL: https://www.sciencedirect.com/science/article/pii/S0013468617304838.

[52] Xinrong Huang et al. "A Review of Pulsed Current Technique for Lithium-ion Batteries". In: *Energies* 13 (May 2020), p. 2458. DOI: 10.3390/en13102458.

[53] Masatoshi Uno and Koji Tanaka. "Influence of High-Frequency Charge–Discharge Cycling Induced by Cell Voltage Equalizers on the Life Performance of Lithium-Ion Cells". In: *IEEE Transactions on Vehicular Technology* 60.4 (2011), pp. 1505–1515. DOI: 10.1109/TVT.2011.2127500.

[54] Sandrine Bourlot, Philippe Blanchard, and Stéphanie Robert. "Investigation of aging mechanisms of high power Li-ion cells used for hybrid electric vehicles". In: *Journal of Power Sources* 196.16 (2011). 15th International Meeting on Lithium Batteries (IMLB), pp. 6841–6846. ISSN: 0378-7753. DOI: https://doi.org/10.1016/j.jpowsour.2010.09.103. URL: https://www.sciencedirect.com/science/article/pii/S0378775310017106.

[55] Thomas B. Reddy David Linden. *Handbook of batteries*. 3rd ed. Aug. 2001, p. 1454.

[56] Manh-Kien Tran et al. "Comparative Study of Equivalent Circuit Models Performance in Four Common Lithium-Ion Batteries: LFP, NMC, LMO, NCA". In: *Batteries* 7 (July 2021), p. 51. DOI: 10.3390/batteries7030051.

[57] Liang-Rui Chen. "A Design of an Optimal Battery Pulse Charge System by Frequency-Varied Technique". In: *Industrial Electronics, IEEE Transactions on* 54 (Mar. 2007), pp. 398–405. DOI: 10.1109/TIE.2006.888796.

[58] Liang-Rui Chen. "Design of Duty-Varied Voltage Pulse Charger for Improving Li-Ion Battery-Charging Response". In: *Industrial Electronics, IEEE Transactions on* 56 (Mar. 2009), pp. 480–487. DOI: 10.1109/TIE.2008.2002725.

[59] Xiao-Guang Yang et al. "Modeling of lithium plating induced aging of lithium-ion batteries: Transition from linear to nonlinear aging". In: *Journal of Power Sources* 360 (2017), pp. 28–40. ISSN: 0378-7753. DOI: https://doi.org/10.1016/j.jpowsour.2017.05.110. URL: https://www.sciencedirect.com/science/article/pii/S0378775317307619.

[60] Alexander C Kozen et al. "Next-Generation Lithium Metal Anode Engineering via Atomic Layer Deposition". In: *ACS nano* 9.6 (June 2015), pp. 5884–5892. ISSN: 1936-0851. DOI: 10.1021/acsnano.5b02166. URL: https://doi.org/10.1021/acsnano.5b02166.

[61] Karen E. Thomas and John Newman. "Thermal modeling of porous insertion electrodes". In: *Journal of the Electrochemical Society* 150.2 (2003). Cited by: 277, A176–A192. DOI: 10.1149/1.1531194. URL: https://www.scopus.com/inward/record.uri?eid=2-s2.0-

0037324033&doi=10.1149%2f1.1531194&partnerID=40&md5=2d285582694a84ae14d6ede73cc119db.

[62] Tequipment. *Chroma 63103A - Load Module 60A/80V/300W*. Nov. 2023. URL: https://www.tequipment.net/Chroma/63103A/Electronic-Loads/.

[63] Maxwell Woody et al. "Strategies to limit degradation and maximize Li-ion battery service lifetime - Critical review and guidance for stakeholders". In: *Journal of energy storage* 28 (2020), p. 101231.

[64] J. Li, R.G. Landers, and J. Park. "A comprehensive single-particle-degradation model for battery state-of-health prediction". In: *Journal of Power Sources* 456 (2020), p. 227950. ISSN: 0378-7753. DOI: https://doi.org/10.1016/j.jpowsour.2020.227950. URL: https://www.sciencedirect.com/science/article/pii/S0378775320302536.

[65] Yu Merla et al. "Novel application of differential thermal voltammetry as an in-depth state-of-health diagnosis method for lithium-ion batteries". In: *Journal of Power Sources* 307 (Mar. 2016), pp. 308–319. DOI: 10.1016/j.jpowsour.2015.12.122.

[66] Victor Agubra and Jeffrey Fergus. "Lithium Ion Battery Anode Aging Mechanisms". In: *Materials* 6 (Mar. 2013), pp. 1310–1325. DOI: 10.3390/ma6041310.

[67] Thomas Waldmann et al. "Temperature dependent ageing mechanisms in Lithium-ion batteries – A Post-Mortem study". In: *Journal of Power Sources* 262 (2014), pp. 129–135. ISSN: 0378-7753. DOI: https://doi.org/10.1016/j.jpowsour.2014.03.112. URL: https://www.sciencedirect.com/science/article/pii/S0378775314004352.

[68] Cheng Lin et al. "Aging Mechanisms of Electrode Materials in Lithium-Ion Batteries for Electric Vehicles". In: *Journal of Chemistry* 2015 (June 2015). DOI: 10.1155/2015/104673.

[69] J. Vetter et al. "Ageing mechanisms in lithium-ion batteries". In: *Journal of Power Sources* 147.1 (2005), pp. 269–281. ISSN: 0378-7753. DOI: https://doi.org/10.1016/j.jpowsour.2005.01.006. URL: https://www.sciencedirect.com/science/article/pii/S0378775305000832.

[70] Shigeomi Takai et al. "Diffusion coefficient measurement of lithium ion in sintered Li1.33Ti1.67O4 by means of neutron radiography". In: *Solid State Ionics* 123.1 (1999), pp. 165–172. ISSN: 0167-2738. DOI: https://doi.org/10.1016/S0167-2738(99)00095-8. URL: https://www.sciencedirect.com/science/article/pii/S0167273899000958.

[71] Yan-Bing He et al. "Gassing in Li4Ti5O12-based batteries and its remedy". In: *Scientific reports* 2 (Dec. 2012), p. 913. DOI: 10.1038/srep00913.

[72] Xiao-Guang Yang et al. "A look into the voltage plateau signal for detection and quantification of lithium plating in lithium-ion cells". In: *Journal of Power Sources* 395 (2018), pp. 251–261. ISSN: 0378-7753. DOI: https://doi.org/10.1016/j.jpowsour.2018.05.073. URL: https://www.sciencedirect.com/science/article/pii/S0378775318305573.

[73] B. K. Purushothaman and U. Landau. "Rapid Charging of Lithium-Ion Batteries Using Pulsed Currents: A Theoretical Analysis". In: *Journal of The Electrochemical Society* 153.3 (Jan. 2006), A533. DOI: 10.1149/1.2161580. URL: https://dx.doi.org/10.1149/1.2161580.

[74] Clement Bommier et al. "In Operando Acoustic Detection of Lithium Metal

Plating in Commercial LiCoO2/Graphite Pouch Cells". In: *Cell Reports Physical Science* 1.4 (2020), p. 100035. ISSN: 2666-3864. DOI: https://doi.org/10.1016/j.xcrp.2020.100035. URL: https://www.sciencedirect.com/science/article/pii/S2666386420300254.

[75] Xinchen Zhao et al. "Electrochemical-thermal modeling of lithium plating/stripping of Li(Ni0.6Mn0.2Co0.2)O2/Carbon lithium-ion batteries at subzero ambient temperatures". In: *Journal of Power Sources* 418 (2019), pp. 61–73. ISSN: 0378-7753. DOI: https://doi.org/10.1016/j.jpowsour.2019.02.001. URL: https://www.sciencedirect.com/science/article/pii/S0378775319301119.

[76] Zhe Li et al. "A review of lithium deposition in lithium-ion and lithium metal secondary batteries". In: *Journal of Power Sources* 254 (2014), pp. 168–182. ISSN: 0378-7753. DOI: https://doi.org/10.1016/j.jpowsour.2013.12.099. URL: https://www.sciencedirect.com/science/article/pii/S0378775313020880.

[77] Qiang Shi et al. "Robust solid/electrolyte interphase on graphite anode to suppress lithium inventory loss in lithium-ion batteries". In: *Carbon* 111 (Oct. 2016). DOI: 10.1016/j.carbon.2016.10.008.

[78] Wei-Jun Zhang. "A review of the electrochemical performance of alloy anodes for lithium-ion batteries". In: *Journal of Power Sources* 196.1 (2011), pp. 13–24. ISSN: 0378-7753. DOI: https://doi.org/10.1016/j.jpowsour.2010.07.020. URL: https://www.sciencedirect.com/science/article/pii/S0378775310011699.

[79] Hui Wu et al. "Stable cycling of double-walled silicon nanotube battery anodes through solid–electrolyte interphase control". In: *Nature Nanotechnology volume* 7 (2012), pp. 305–315. DOI: 10.1038/nnano.2012.35.

[80] Uday Kasavajjula, Chunsheng Wang, and A. Appleby. "Nano- and Bulk-Silicon-Based Insertion Anodes for Lithium-Ion Secondary Cells". In: *Journal of Power Sources* 163 (Jan. 2007), pp. 1003–1039. DOI: 10.1016/j.jpowsour.2006.09.084.

[81] Izaro Laresgoiti et al. "Modeling mechanical degradation in lithium ion batteries during cycling: Solid electrolyte interphase fracture". In: *Journal of Power Sources* 300 (Dec. 2015), pp. 112–122. DOI: 10.1016/j.jpowsour.2015.09.033.

[82] Taina Rauhala et al. "Low-temperature aging mechanisms of commercial graphite/LiFePO4 cells cycled with a simulated electric vehicle load profile—A post-mortem study". In: *Journal of Energy Storage* 20 (2018), pp. 344–356. ISSN: 2352-152X. DOI: https://doi.org/10.1016/j.est.2018.10.007. URL: https://www.sciencedirect.com/science/article/pii/S2352152X18303694.

[83] Cheng Lin et al. "Aging Mechanisms of Electrode Materials in Lithium-Ion Batteries for Electric Vehicles". In: *Journal of Chemistry* 2015 (June 2015). DOI: 10.1155/2015/104673.

[84] Wei-Jun Zhang. "Structure and performance of LiFePO4 cathode materials: A review". In: *Journal of Power Sources* 196.6 (2011), pp. 2962–2970. ISSN: 0378-7753. DOI: https://doi.org/10.1016/j.jpowsour.2010.11.113. URL: https://www.sciencedirect.com/science/article/pii/S037877531002104X.

[85] Li Wang et al. “Insights for understanding multiscale degradation of LiFePO4 cathodes”. In: *eScience* 2 (Mar. 2022). DOI: 10.1016/j.esci.2022.03.006.

[86] Dervis Emre Demirocak and Bharat Bhushan. “Probing the aging effects on nanomechanical properties of a LiFePO4 cathode in a large format prismatic cell”. In: *Journal of Power Sources* 280 (2015), pp. 256–262. ISSN: 0378-7753. DOI: https://doi.org/10.1016/j.jpowsour.2015.01.114. URL: https://www.sciencedirect.com/science/article/pii/S0378775315001305.

[87] Vallabha Rao Rikka et al. “Temperature-Derived Fe Dissolution of a LiFePO4/Graphite Cell at Fast Charging and High State-of-Charge Condition”. In: *Energy Technology* (Mar. 2023). DOI: 10.1002/ente.202201388.

[88] K. Amine, J. Liu, and I. Belharouak. “High-temperature storage and cycling of C-LiFePO4/graphite Li-ion cells”. In: *Electrochemistry Communications* 7.7 (2005), pp. 669–673. ISSN: 1388-2481. DOI: https://doi.org/10.1016/j.elecom.2005.04.018. URL: https://www.sciencedirect.com/science/article/pii/S1388248105001177.

[89] Maik Naumann et al. “Analysis and modeling of calendar aging of a commercial LiFePO4/graphite cell”. In: *Journal of Energy Storage* 17 (2018), pp. 153–169. ISSN: 2352-152X. DOI: https://doi.org/10.1016/j.est.2018.01.019. URL: https://www.sciencedirect.com/science/article/pii/S2352152X18300665.

[90] C. Delacourt and M. Safari. “Life Simulation of a Graphite/LiFePO4 Cell under Cycling and Storage”. In: *Journal of The Electrochemical Society* 159.8 (July 2012), A1283. DOI: 10.1149/2.049208jes. URL: https://dx.doi.org/10.1149/2.049208jes.

[91] Johannes Kasnatscheew et al. “Learning from electrochemical data: Evaluation and classification of LiMO2 type based positive electrodes for Li ion batteries by using a novel electrochemical analysis methodology”. In: *Energy Technology* 5 (Mar. 2017). DOI: 10.1002/ente.201700068.

[92] Aleksandr Kondrakov and Alexander Schmidt. “On the Anisotropic Lattice Strain and Mechanical Degradation of High- and Low-Nickel NCM Cathode Materials for Li-Ion Batteries”. In: *The Journal of Physical Chemistry C* 121 (Jan. 2017), p. 17. DOI: 10.1021/acs.jpcc.6b12885.

[93] Byung-Beom Lim et al. “Advanced Concentration Gradient Cathode Material with Two-Slope for High-Energy and Safe Lithium Batteries”. In: *Advanced Functional Materials* 25 (Aug. 2015). DOI: 10.1002/adfm.201501430.

[94] Ho-Hyun Sun and Arumugam Manthiram. “Impact of Microcrack Generation and Surface Degradation on a Nickel-Rich Layered Li[Ni0.9Co0.05Mn0.05]O2 Cathode for Lithium-Ion Batteries”. In: *Chemistry of Materials* 29 (Sept. 2017). DOI: 10.1021/acs.chemmater.7b03268.

[95] Hyejung Kim et al. “A New Coating Method for Alleviating Surface Degradation of LiNi0.6Co0.2Mn0.2O2 Cathode Material: Nanoscale Surface Treatment of Primary Particles”. In: *Nano Letters* 15.3 (2015). PMID: 25668708, pp. 2111–2119. DOI: 10.1021/acs.nanolett.5b00045. eprint: https://doi.org/10.1021/acs.nanolett.5b00045. URL: https://doi.org/10.1021/acs.nanolett.5b00045.

[96] Manuel Weiß et al. “Fast Charging of Lithium-Ion Batteries: A Review of Materials Aspects”. In: *Advanced Energy*

Materials 11 (July 2021). DOI: 10.1002/aenm.202101126.

[97] Martin Winter, Brian Barnett, and Kang Xu. "Before Li Ion Batteries." In: *Chemical reviews* 118 23 (2018), pp. 11433–11456.

[98] Andreas Nyman, Mårten Behm, and Göran Lindbergh. "Electrochemical characterisation and modelling of the mass transport phenomena in LiPF6-EC-EMC electrolyte". In: *Electrochimica Acta - ELECTROCHIM ACTA* 53 (Sept. 2008), pp. 6356–6365. DOI: 10.1016/j.electacta.2008.04.023.

[99] Richard Jow et al. "Factors Limiting Li + Charge Transfer Kinetics in Li-Ion Batteries". In: *Journal of The Electrochemical Society* 165 (Jan. 2018), A361–A367. DOI: 10.1149/2.1221802jes.

[100] Chong Yan et al. "Nucleation and Growth Mechanism of Anion-Derived Solid Electrolyte Interphase in Rechargeable Batteries". In: *Angewandte Chemie International Edition* 60.15 (2021), pp. 8521–8525. DOI: https://doi.org/10.1002/anie.202100494. eprint: https://onlinelibrary.wiley.com/doi/pdf/10.1002/anie.202100494. URL: https://onlinelibrary.wiley.com/doi/abs/10.1002/anie.202100494.

IX. Appendix

***Abstract*— Understanding the degradation processes of lithium-ion batteries is crucial for further development of high-performance lithium-ion batteries. The paper highlights the four main causes of degradation: the growth of the solid electrolyte interface (SEI) layer, lithium plating, cathode metal dissolution, and particle cracking and fracturing. From the user's perspective, degradation presents itself as capacity fade and or power fade, which are caused by three main degradation modes; loss of lithium inventory, loss of active material, and impedance increase. This paper is made to give a comprehensive overview of research into done on the degradation processes within lithium-ion batteries. It highlights the interconnected nature of degradation processes and emphasizes the potential for optimizing the electrolyte and employing advanced manufacturing techniques to enhance cell performance and prolong cycle life.**

A. Introduction

Over the past decade, there has been a significant surge in interest in lithium-ion battery technology, primarily driven by its potential in combating climate change and reducing reliance on fossil fuels, particularly in the automotive industry. This heightened interest has spurred remarkable advancements in the technology, with the development of larger and higher density battery packs aimed at pushing the boundaries of battery performance forward.

The shift from fossil fuel-based power to electric power has stimulated the development and research into gaining in-depth knowledge of electrochemical processes and the overall mechanisms surrounding the functioning of batteries, especially lithium-ion batteries. Extensive amount of reports and studies have be conducted surrounding the degradation of the batteries in pursuit to increase the overall lifetime of the cells. The shear size of papers surrounding the complicated and multidisciplinary topic of battery degradation makes fully understanding and learning the mechanisms of degradation time consuming and difficult. This paper is aimed at delivering the present knowledge of the scientific community in one comprehensive paper to limit the amount of studies and documents that needs to be read in order to comprehend the topic at hand.

Different review papers have already done this work in their own fields. J. P. Pender *et al.* [15] has done this in the field of electrochemistry in the scope of different electrode materials and their challenges. Woody *et al.* [63] has refined the effects of best practise use of LIB and how the lifetime of li-ion batteries can be extended by looking at the State of Health (SoH) deterioration over a range of user-defined parameters. J. Li *et al.* [64] elaborated on this knowledge by creating a single particle physical model which was able to predicted the capacity fade over time. Other models, significantly reduce computational requirements by relying on empirical data-driven approaches.

The purpose of this paper is to summarize the main points and findings of these papers, among others, in order to present a clear picture of the current state of degradation research.

B. Battery Cell Characteristics: Setting the Foundation

Overall a battery cell can be broken down to four elements the anode, the cathode, the electrolyte and the separator. Furthermore can the anode and cathode be sub sectioned into the electrode material, the binder and the current collector. Figure 18 shows these elements in detail and how the interact with each other.

The electrode with the highest potential is mostly referred to as the cathode of the cell (connected to the positive terminal), while the electrode with the lowest potential is referred to the anode (connected to the negative terminal). Of mostly used lithium-ion batteries, the positive electrode referred to as the cathode is typically built out of transition metal oxide material that can undergo reversible delithiation. Significant research has been conducted in the field of cathode material design, given its substantial impact on the overall energy density of the cell. According to P.J. Pender et al. [15], the cathode accounts for approximately 41% of the total weight of the cell, thus significantly impacting energy density.

The second electrode consist typically out of graphite or carbon composites which can intercalate lithium-ions and is referred to as the anode. Substantial research is also conducted in

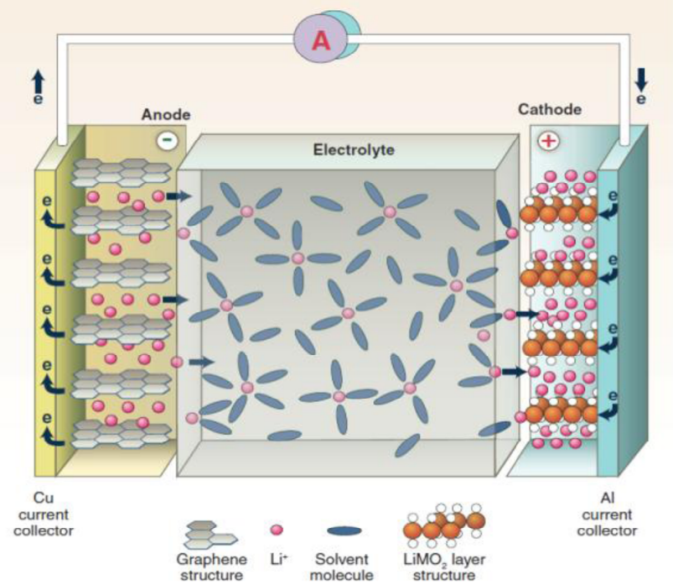

Fig. 18: Diagram illustrating the layout of the primary components that comprise a battery. [16]

this domain due to the intrinsic nature of the anode and the degradation process resulting from the formation of the Solid Electrolyte Interface (SEI) layer which forms between the active material of the anode and the electrolyte [34]. Other promising candidates for anode materials are silicon, soft carbon, graphene and lithium titanium oxide (LTO).

Both electrodes are coated on a metal conducting current collector connected to the terminals of the cell, with the help of a binder material which acts as the glue between the active material and the current collector and allows for good electrical connectivity. On the cathode the current collector material is aluminum while the anode uses a sheet of copper to conduct the current to the terminals. This difference is material is required to the electrochemical potential of both material, with aluminum having a higher potential and thus more stable against the higher potential of the cathode, avoiding unwanted redox reaction between the cathode active material and the current collector. Within the cell, during the charging process, lithium-ions are delithiated from the cathode's structure and migrate towards the anode. At the anode, the Li^+ ions undergo lithiation into the graphite and recombine with electrons that have traveled trough the external connected load.

In the discharge setting, the opposite reaction

takes place, allowing for the delithiation of the Li^+ ions in the anode and the lithiation inside the cathodes crystalline structure. The active materials in both electrodes must be capable of intercalating Li^+ ions over multiple cycles. The ability of these active materials to undergo lithiation and delithiation reactions, as well as their response to the associated mechanical and chemical stresses while maintaining crystal stability throughout these cycles, significantly impacts the cycle life of the battery.

The challenge in electrode material development lies in the ability of the active material to keep its functionality over multiple cycles, while at the same time achieving high energy and power density and also maintaining mechanical, chemical, and thermodynamic stability.

The two electrodes are isolated from each other by a separator in between the electrodes, which allows the transport of ions but acts as a barrier for electrons. These layers are in most commercial batteries drown in a liquid electrolyte which enables fast ionic transfer between the two electrodes.

C. Exploring the causes of degradation

The degradation process of batteries can be divided into two noticeable main parts; capacity fade and power fade. Both have their own underlying causes, which are also depended on each other. Looking at the characterizing degradation phenomenons, three main modes can be distinguished.

1) The Loss of Active Material (LAM), which refers to the mechanisms that reduce the amount of active material available for the electrochemical intercalation reaction of lithium. These mechanisms include side reactions that occur in the cell, leading to a decrease in the active material capable of participating in the reaction on both the current collectors and the electrolyte.

2) The Loss of Lithium Inventory (LLI), which refers to the mechanisms that decrease the amount of lithium-ions available to participate in the intercalation and delithiation cycle process. These mechanisms result in a reduction in the available lithium-ions for the electrochemical reactions.

3) The increase in internal impedance of the cell, which refers to the mechanisms that hinder the transport of ions between the electrodes and the increased electrical resistance of the current collectors. These mechanisms lead to an overall increase in the internal impedance of the cell, affecting, typically, its power performance, leading to power fade.

All three main characterized phenomena are interlinked with each other, making the degradation of lithium-ion cells a complex endeavor. To begin explaining the degradation, we first examine the anode, which is typically strongly affected by the formation and growth of the Solid Electrolyte Interface (SEI), as well as lithium plating. Next, we explore the cathode, where similar processes occur, including the formation of SEI and dissolution of transition metals into the electrolyte, which can have a cascading effect on the anode's SEI formation. Finally, we consider the mechanical stress and its impact on the cell's performance while assessing any potential negative or positive feedback loops that interconnect the degradation mechanisms with each other.

D. Anode material

1) SEI layer formation: The formation of the SEI layer on the anode refers to the layer that develops on the surface of the electrode, typically graphite, as a result of the interaction between the pristine graphite and the electrolyte. The organic electrolyte used is typically the salt $liPF_6$ combined with other solvents, namely ethylene carbonate (EC), dimethyl carbonate (DMC), diethyl carbonate (DEC), and methyl ethyl carbonate (EMC) [66]. Graphite creates a potential with 0.2V versus lithium, which is advantageous due to its positive impact on the cell's operating potential. However, this potential also poses a challenge as it increases the risk of electrochemical instability of the electrolyte which becomes unstable at potentials below 1.0V [34]. This low potential of graphite allows for the occurrence of electrochemical side reactions due to the decomposition of the electrolyte, leading to the formation of various inorganic and organic compounds on the graphite surface [67]. If the

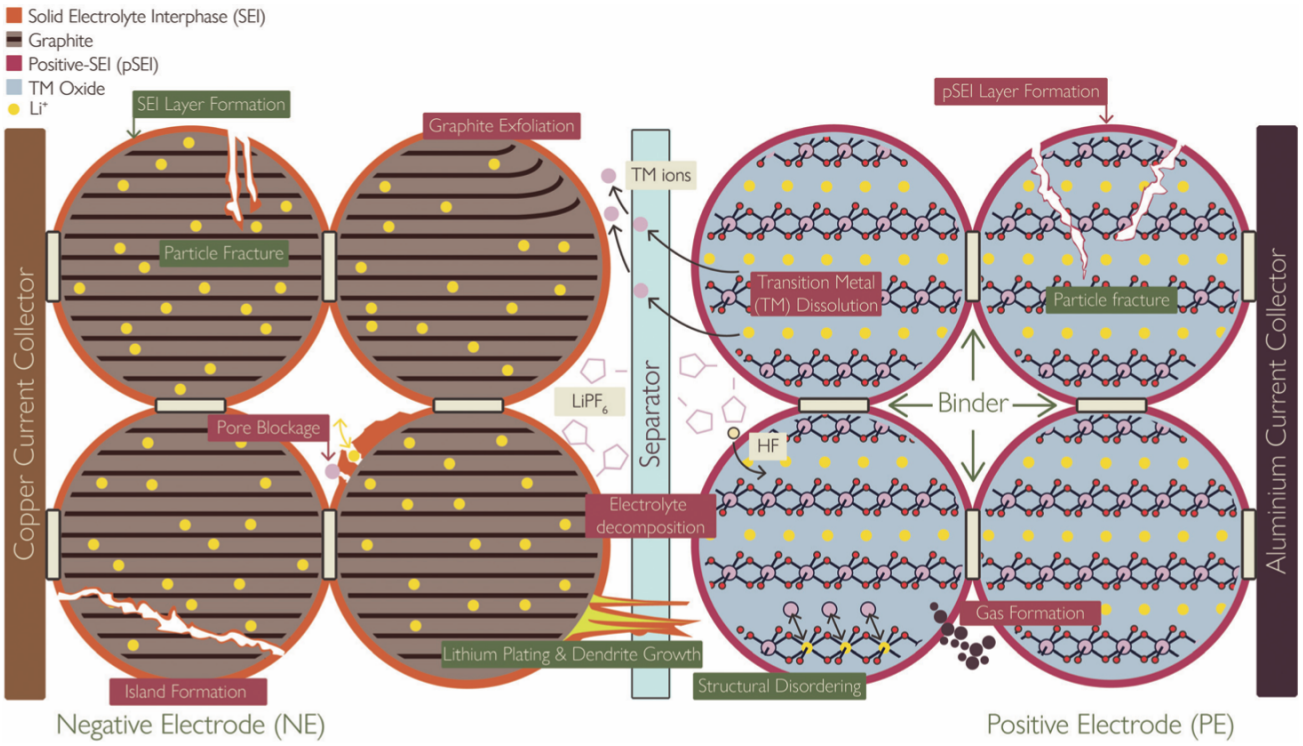

Fig. 19: This figure provides an overview of the most significant degradation mechanisms occurring inside lithium-ion batteries (LIBs).The most pressing processes are indicated in green, while the additional mechanisms are shown in dark red.[65][3].

anode operates outside the electrochemically stable window of the electrolyte, the $liPF_6$ solvents will react strongly with EC and DMC, resulting in the production of gases (CO_2, CO, and H_2) within the cell. Additionally, ionically conductive but electrically insulating particles will form and bond to the surface of the anode [68]. These particles consist of, among other out of lithium carbonate ($LiCO_3$), lithium ethylene dicarbonate $(CH_2OCO_2Li)_2$, lithium methyl carbonate (CH_3OCO_2Li), lithium oxide (Li_2O), and lithium fluoride (LiF) [69].

During the initial formation of the SEI layer, the reactions are highly aggressive and rapid. According to studies approximately 10% of the lithium-ion capacity of the cell is lost during the first cycle due to the rapid formation and consumption of lithium-ions on the electrode surface [3]. Following this initial cycle, the SEI layer acts as a protective barrier between the electrolyte and the graphite, effectively slowing down the process of SEI formation. The process can be compared to the oxidation reaction with oxygen on the surface of pristine aluminium, protecting the aluminium from further oxidation deeper in the material.

Nevertheless, in lithium-ion cells, the protective layer of SEI formed during the first cycle is not entirely adequate to completely prevent the growth of SEI, and over time, the SEI layer is prone to grow. This mechanism occurs due to various factors;

Firstly, the exposure of a new pristine graphite surface to the electrolyte resulting from mechanical stress caused by the volume changes between the lithiation and delithiation states of the graphite electrode. When the anode is lithiated, the overall volume of graphite containing the lithium-ions expands to accommodate the space for the lithium-ions. During delithiation, the graphite layers contract again, reducing the volume they occupy. The cycling of a cell, therefore, introduces mechanical stress due to the contraction and expansion of the graphite structure, resulting in cracks in the SEI layer on the surface of the graphite. These cracks open up

new fresh graphite to the electrolyte, allowing the SEI layer to grow again.

Additionally, solvent molecules from the electrolyte can diffuse through the present SEI layer and reach the graphite. The solvents will come into contact with the graphite and due to its low potential will react with it to create further SEI layer compounds.

Furthermore, the dissolution of transition metals from the cathode, along with the build up of lithium-ions (lithium plating) on the surface of the SEI layer, can further contribute to the increased formation of SEI on top of these metal deposition.

The growth of this SEI layer, by the decomposition process of the electrolyte at the anode surface, does not only contribute to the loss of lithium, but also increases ionic transfer resistance and therefore increasing the overall impedance of the cell. Consequently, SEI layer composition affects to both capacity fade and power fade.

The fact that SEI grows due to decomposition of the electrolyte at low potentials, explains why Lithium Titanate Oxide (LTO) has gained traction in the battery domain. The strong crystal structure and consequently its low volume change during lithiation and delithiation, combined with its relatively high operating potential that falls within the stable voltage windows of commonly used electrolytes, make this anode material mechanically and chemically stable [34]. As a result, the rate of SEI formation on the surface is strongly reduced, leading to lower capacity- and power fade over time. However, it must be said that the higher operating potential of the LTO anode also comes with a drawback: it leads to a lower cell operating voltage, which therefore reduces its energy density. Another issue is the excessive amount of gas formation and the relatively low lithium-ion diffusion speed inside the LTO crystals makes the anode material still challenging [70] [71].

2) Lithium plating: Lithium plating is referred to the reaction of lithium-ions deposition into metallic lithium on the surface of the electrode. This phenomenon mainly takes place at the anode during lithiation. The reaction typically takes place when the rate of intercalaction into the graphite lattice is lower than the charging rate, resulting in an excess of lithium-ions that plate onto the surface of the anode[72] [73]. Lithium plating can occur when the cell is charged at low temperatures, which leads to slow charge transfer kinetics and low diffusion of lithium-ions. The low potential of graphite to that of lithium (0.1 V Vs li^+/Li) makes lithium susceptible to plating [74]. Additionally, a high state of charge (SoC) or even over-charging the cell increases the likelihood of lithium plating due to the lower intercalation speed into the lattice, which is caused by the increased path resistance of the lithium-ions into the graphite at higher SoC [75]. The SEI layer is conductive for lithium-ions but restive to electrons. Because of this, lithium plating can only occur between the interface of the graphite and the SEI layer [76]. During discharge the plated lithium can undergo a process called *stripping* in which the electrons are stripped from the metallic lithium and lithium-ions are diffused back into the electrolyte.

This process forms the basis of a fully metallic lithium anode, which increases the energy density to the theoretical capacity of 3860 mAh/g while having the lowest electrochemical potential [15]. However, challenges persist regarding the extreme reactivity of lithium with traces of moisture and its reaction with the electrolyte, leading to the formation of an SEI layer, which remains an unsolved challenge [60]. Promising research is done in this field which uses atomic layer deposition (ALD) to create a protection layer out of Al_2O_3 directly on Li metal with exquisite thickness control to limit the SEI formation on the surface [15] [60]. In this study, a 2 nm thick layer was deposited on the electrode active material which improved the cycle life with 250%.

The plated lithium in graphite-based batteries, can further react with the electrolyte to form a secondary SEI layer before a discharge is applied to the cell. This layer traps the lithium metal, preventing it from accessing its sources of electrons and undergoing an oxidation reaction. This trapped lithium is referred to as dead

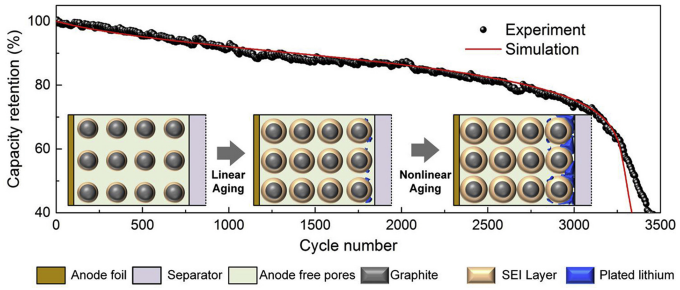

Fig. 20: The schematic illustration depicts the aging behavior of a cell undergoing prolonged cycling, transitioning from linear to nonlinear aging over time due to the onset of lithium plating [59].

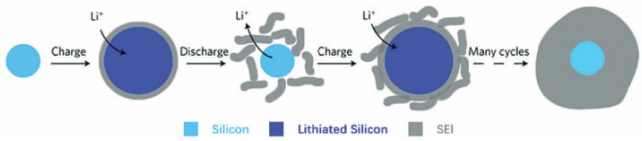

Fig. 21: The schematic illustration shows the constant buildup of SEI layer compositions on the surface of silicon particles during the excessive volume change between the lithiated and delithiated states [79].

lithium since it no longer contributes to the battery's operation, leading to irreversible capacity fade. Not only lithium-ions are consumed during this, the formation of the secondary SEI layer also consumes electrolyte solvents as well and contribute to pore clogging of the anode, which again will increasing the impedance of the cell [72]. The rate of lithium plating can be influenced by the electrolyte composition. A study conducted by Shi *et al.* demonstrated that electrolyte solvents based on EC are more prone to lithium plating compared to other solvent mixtures [77].

Another factor that influences the growth of dendrites and lithium plating is the purity and order of the graphite structure. Any contamination or disorder will negatively affect the homogeneous current distribution, which, in turn, leads to high local concentrations of lithium-ions, increasing the probability of plating.

Studies surrounding the degradation patterns suggest that the capacity fade occurs quite linearly with the number of cycles up to the point where lithium plating becomes more dominant, increasing the degradation to a non-linear slope [3]. This is due to the hypothesis of the existing positive feedback process of SEI growth and lithium plating, which accelerates the capacity degradation to a non-linear manner, seen in figure 20[59].

3) Anode mechanical degradation: As stated before, the main mechanisms of degradation inside a lithium-ion battery are due to the loss of lithium inventory (LLI), loss of active material (LAM), and increased impedance. Lithium-ions can be consumed during the formation of the SEI layer, as well as the formation of metallic metal composition in the form of dead lithium. Increased impedance can be attributed to the increased thickness of the SEI layer, the decrease in solvents due to their consumption into the SEI layer, and the clogging of the pores for lithium-ions in the graphite structure, resulting in increased resistance, which occurs with lithium plating. However, loss of active material is not yet described in detail. Another mechanism that decreases the cell's capacity and power performance is due to the loss of active material due to particle cracking. As mentioned before, volume expansion can fracture SEI layer compositions, exposing fresh graphite. However, the active materials on both electrodes can also crack and fracture due to this volume expansion during cycling. Heterogeneous current distributions can not only lead to an increased chance of lithium plating but also increase the local stress on the active material, resulting in fragmentation and eventually pulverization of the electrode materials, which will again lead to capacity and power fade.

This effect is particularly severe with silicon based anodes. Although the theoretically specific capacity of silicon is extremely high (4200 mAh/g) [78], the stresses caused by its 300%-400% volume expansion during lithiation and delithiation states are problematic. This expansion comes with the price of low cycle life and high initial capacity fade. A schematic figure showing this process is shown in figure 21, reprinted by Wu *et al.* [79] The cracking and fracturing of the active material can electrically isolate certain parts from the current collector, reducing the amount of active material available for the cycling intercalation reactions

as well as trapping lithium-ions, resulting in capacity fade [80]. This effect is proven to be directly related to each other by Laresgoiti *et al.* [81] who showed that capacity fade was directly proportional to the amount of mechanical particle stress.

Mechanical stress is intensified at higher temperatures, which also brings thermal stress, causing more fracturing and cracking. Additionally, low temperatures can make the graphite brittle, increasing the chance of mechanical failure [82]. Temperature gradients in the cell can further induce heterogeneous current distributions, resulting in more heterogeneous local mechanical stresses. This, in turn, leads to fractures and cracking due to the uneven distribution of mechanical forces.
In addition to the losses of active material and mechanical stress in the active materials, the non-active materials can also experience fatigue. In order to properly coat the active cathode and anode material onto their corresponding current collector material (copper and aluminum), a binder is used to facilitate the appropriate electrical and mechanical connection between the two materials. This binder can also experience decomposition and mechanical stress, leading to delamination of the active material and the current collector. Which in turn increases the electronic pathway resistance, which creates more heat and thus lower cell efficiency. Additionally, decomposition products of the binder can form SEI compounds on the surface, leading to the consumption of lithium-ions in the process and thus leading to capacity fade [83].

E. Cathode material

Although it is thought that the anode is the dominant factor in lithium-ion degradation [3], cathode materials can also have a significant influence on capacity and power fade, and even enhance anode degradation. In contrast to the commonly used anode material like graphite, the choice of cathode material does vary more from battery to battery. The most commonly known cathode materials are layered or spinal metal oxides such as $LiCo_2$ or the even more widely used lithium nickel manganese cobalt $LiNi_xMn_yCo_zO_2$ (NMC) or lithium nickel cobalt aluminium $LiNi_xCo_yAl_zO_2$ (NCA). Another very popular structure nowadays is the olivine crystal called lithium iron phosphate ($LiFePO_4$, LFP). Both have their own advantages but overall NMC has the higher energy density while LFP has a more stable structures allowing for prolonged cycle life and safety.
The NMC cathode-based batteries can differ from each other in terms of the distribution ratio between the metals. Each metal in the NMC cathode material (Nickel, Manganese and Cobalt) has its own unique characteristics, and by mixing them in certain ratios, a cathode material with the desired performance can be created.

F. Degradation LFP cathode material

Lithium Iron Phosphate (LFP) offers advantages compared to layered metal oxide cathodes like NMC or NCA, as it is significantly more stable and robust. This stronger and stable structure comes from the 3D olive structure of the cystral, which harnesses the strong covalent bond (electron sharing of the outer shell) between phosphor and oxygen. For instance, the volume change of LFP between fully lithiated and delithiated states is only 6.77% [84], compared to 12.0% for graphite [85], resulting in lower mechanical stress and therefore less mechanically induced degradation. However, it has a lower specific capacity, and its crystal structure is less conducive to the diffusion of lithium-ions and electrons. These issues have been addressed by nano-structuring the LFP, increasing its surface area, and reducing the diffusion path length for lithium-ions. Additionally, improving its conductivity through the application of a carbon coating has made this material a viable option for commercial lithium-ion batteries.

Through coating and sizing manufacturing processes, the LFP cathode material has almost approached its theoretical limit of 170 mAh/g while maintaining a good cycle life. The cathode material exhibits minimal mechanical degradation due to its strong and stable structure, to the extent that the binder material (PVDF) in commonly used LFP batteries is reported to be a more critical factor in this cathode mechanical degradation [86].

1) Fe^{2+} *dissolution:* Nevertheless, $LiFePO_4$ cathodes still suffer from transition metal

dissolution, similar to NMC cathodes. The Fe ions can dissolve into the electrolyte in the presence of acidic molecules. This 'acid attack' can occur due to trace amounts of moisture in the cell, which react with the electrolyte solvents, resulting in the formation of HF from $LiPF_6$. The HF dissociates into ions of H^+ and F^-. Two H+ ions can replace one Fe^{2+} ion inside a $LiFePO_4$ olive crystal, forming LiH_2PO_4 which can block lithium-ion diffusion into the lattice. The Fe^{2+} ions then dissolve into the electrolyte, either reconciling with an electron to form metallic iron or reacting with the graphite of the anode. If the iron ions dissolve into the electrolyte and migrate to the anode, they form a solid electrolyte interface (SEI) layer by reacting with the graphite. This interaction with Fe^{2+} is likely to occur due to its higher potential (-0.44V vs Lithium) compared to lithium intercalation (-3.04V vs Lithium)[87]. This can lead to capacity fade and the loss of active cathode and anode material. The dissolution of Fe ions is particularly aggravated at elevated temperatures, due to the accelerated generation of H^+ at higher temperatures [88] [87]. According to one study, Fe dissolution and its catalytic effect on SEI layer growth on the anode account for nearly 17%-20% capacity fade compared to the initial capacity [87]. Transition metal dissolution in other cathode materials is different due to the difference in structure between layered materials like NMC and olive structure materials like LFP. The olive structure allows iron dissolution to occur almost exclusively in the presence of traces of moisture, whereas for layered structures, chemical instability during high lithiated or delithiated states can already initiate transition metal dissolution.

Interestingly, looking the other way around, no clear cross-talk between anode degradation and its influence on cathode degradation processes has been found yet [85].

Different methods are employed to limit the dissolution of iron. The use of coatings has been proven effective in lowering the rate of dissolution, as well as optimizing the electrolytes specifically designed for the electrodes used. By optimizing the electrolyte, it becomes possible to address multiple degradation processes, making it an increasingly important area of research.

2) LFP cathode CEI layer formation: The Cathode Electrolyte Interface (CEI) is the SEI equivalent for the cathode, similar to the anode. The voltage curve for LFP-based cells is quite flat, with a plateau voltage of around 3.2V nominal. Due to this lower operating potential compared to NMC or other cathode chemistry's, it remains in the stable voltage region of the electrolyte. However, just as small amounts of water still evaporates below 100°C, small quantities of electrolyte will still reacts with the LFP crystals, forming a CEI layer. This process can be aggravated by iron dissolution. High temperatures, even during storage, can also lead to increased SEI and CEI layer formation, resulting in the consumption of lithium-ions. During high-temperature cycling, phase-changing structures were observed at the surface of the cathode. Thickening layers of amorphous $LiFePO_4$ were found, which increased the ionic transfer resistance and lowered the capacity of the active cathode material to store lithium-ions. High state of charge (SOC) further exacerbates this thickening of such an amorphous layer effect during storage [89]. Although calendar aging can lead to capacity fade and degradation, it is estimated that this effect accounts for 10% to 30% in comparison to cycle-induced aging [90]. While low temperatures remain a concern for the graphite based anode electrodes due to lithium plating, this phenomenon has not been observed at the LFP cathode surface during post-modem analysis [82].

3) LFP cathode mechanical degradation: Although the crystal structure of the LFP in the olive orientation is strong, mechanical stress can still degrade the cell. Inhomogeneous current distribution can heat up specific local parts of the cathode, inducing higher thermal and mechanical local stress gradients. This leads to cracking and fracturing of the active material, binder, or CEI layer. Consequently, this can result in accelerated cell degradation due to the loss of lithium-ions during new CEI formation and the loss of active material due to electrically detachment of the LFP crystal from the current collector.

4) Degradation NMC cathode material : NMC based batteries experience the same chemical degradation processes as LFP cathodes. However, NMC has a weaker, more unstable crystal structure, allowing for a different process of transition metal dissolution and more stress induced cracking can be observed. During lithiation and delithiation, the lattice structure of NMC-based cathodes can undergo a phase change from a layered structure to a disordered spinel or even rock salts [3]. These crystal structural changes not only induce mechanical stress inside the lattice, resulting in cracking and fracturing of the active material, but the transition metals (Nickel, Manganese, and Cobalt) can also dissolute and form a passivating solid layer on the surface of the electrodes, CEI and SEI layer formation. This solid layer consumes lithium-ions and releases oxygen bonds in the process. The released oxygen ions in this process of metal dissolution, quickly react with the carbonated solvents in the electrolyte, leading to the decomposition of the solvents and the formation of gaseous oxygen, carbon dioxide, and other gases. Therefore the active material of cathode, as well as the inventory of lithium and electrolyte as reduced in the process.

The collapse and subsequent phase change in the crystalline structure of NMC based batteries, occur due to the oxidation of Ni^{2+} to Ni^{3+} and even Ni^{4+}. The Ni^{3+} and Ni^{4+} ions can migrate within the structure, occupying Li^{+} sites, which obstructs the pathway and reduces the cathode's capacity to store lithium-ions. This effect is referred to as the Jahn-Teller effect, where an ion is occupying a different site due to distortion leading to instability inside the lattice [15]. The strongly oxidized ions,Ni^{3+} and Ni^{4+}, can also interact rapidly with the electrolyte or undergo a reduction reaction with lattice oxygen ions, resulting in the formation of oxygen gas and Ni^{2+} ions. The oxygen gas can react and degraded the electrolyte further. All the pro's and cons of each the transition metal inside a NMC crystal structure are summarized by in figure 22 [91].

Interestingly, the combination of manganese ions with nickel demonstrates greater thermal and chemical stability in their structure compared to solely nickel oxide or manganese oxide structures. However, incorporating manganese and nickel into the cathode material induces the ion mixing of nickel within the structure, referred to as the Jahn-Teller effect of distortion inside the lattice. Also, manganese tends to dissolve out of the structure and form solid electrolyte interface (SEI) and cathode-electrolyte interface (CEI) layers when it comes into contact with the electrolyte, especially at high temperatures and high states of charge (SOC).

By incorporating cobalt into the cathode material, the dissolution of manganese is limited, while overall stability of the lattice is enhanced. It is worth noting that cobalt is not the only element capable of delivering this stability; iron, for example, exhibits similar capabilities when mixed with nickel and manganese. However, the addition of cobalt significantly boosts energy density by enabling a higher cathode potential, making it an attractive choice. However, it does have its drawback, which is the instability of organic electrolytes at high potentials, typically above approximately 4.2 V [15].

The interest in nickel-rich cathodes stems from its high energy density and the ethical concerns surrounding cobalt mining. However, it has been observed that higher ratios of nickel content lead to greater volumetric changes and increased oxygen release due to nickel mixing and disordering of the lattice structure, resulting in the formation of rock salts [92]. Consequently, several interesting studies have been conducted to optimize the nickel content without compromising stability and, consequently, cycle life.

One of these studies aimed to create a nickel-rich core with a nickel ratio of up to 0.9, which was surrounded by a shell composed of manganese and cobalt [93] [94]. The stable properties of manganese and cobalt were utilized to accommodate the high energy capacity of the nickel-rich core. In addition to this, another complementary approach was proposed to protect the nickel and manganese from interactions with the electrolyte and enhance the chemical stability of the lattice, which involved the application of a surface treatment coating [95].

The nickel-rich NMC cathode materials are of interest for high-performance, high-energy-density applications. The increased density is partly attributed to the higher potential of the cathode material. However, the higher potential necessitates considering the electrochemical stability of the organic electrolyte. Commonly encountered electrolytes such as EC, DMC, and MC exhibit stability within the potential range of approximately 1.5 V to 4.2 V [3]. NMC cathodes can achieve higher potentials, exposing them to chemical instability, decomposition, and degradation at these elevated potentials. Consequently, there is growing interest in optimizing the composition of the electrolyte to increase cycle life of the cells.

G. Electrolyte

Currently, there are different types of electrolytes being investigated and used for certain LIB systems. However, organic liquid electrolytes still occupy the sweet spot between performance and cost-effectiveness [97]. The commonly used electrolyte contains approximately 1 mol/L $LiPF_6$ in combination with organic solvents such as EC, DMC, DEC, or EMC. Although the competitive market, especially the EV car industry, constantly pushes the boundaries of energy density, electrolyte innovation has not been a high priority due to its limited impact on cell performance gain. This is because the ionic transfer is not bottlenecked by the ionic conductivity of the electrolyte but rather by the intercalation diffusion kinetics into the electrode lattice, particularly at the anode, to achieve higher charging speeds.

Studies have even shown that reducing the concentration of $LiPF_6$ salt from 1.0 mol/L to 0.2 mol/L does not significantly affect the cell performance [98]. However, the charge-limiting factor is found to be closer to the SEI layer kinetics, leading to further research on shaping this layer with the use of additives in the electrolyte solvents. The SEI layer is composed of solvent compounds, so by tailoring the mixture of molecules in the electrolyte, the characteristics of the SEI layer can be adjusted. For example, it has been found that adding lithium bis(fluorosulfonyl)imide (LiFSI) to the solvent mixture lowers the charge transfer resistance of the SEI layer [99]. Additionally, incorporating more inorganic solvents can help form inorganic compounds in the SEI layer, enabling faster charge transfer and enhancing stability [100].

Although the performance of the cell is not limited by the electrolyte, the electrochemical stability window of the electrolyte, ranging from 1.0 V to 4.2 V, does have an influence on degradation. When the anode potential falls outside this voltage range, $LiPF_6$ starts to react with solvents such as EC and DMC, resulting in the consumption of lithium and electrolyte, as well as the generation of gases. Additionally, this process inherently leads to the growth of the SEI layer. Interestingly, these reactions can also produce H_2O, which can rapidly react with $LiPF_6$ again, forming acidic species like HF. This enables further reactions on the cathode side, leading to the dissolution of transition metals into the electrolyte and, in turn, promoting SEI growth on the anode.

This interconnected chain of processes illustrates the complexity and intertwined nature of battery degradation; Almost all processes and reactions are interconnected and influence each other. A clear overview of the degradation modes and interconnected effects can be seen in figure 23.

H. Conclusion

In order to understand the essential mechanisms of battery degradation, a significant number of papers have been read and summarized in this paper to consolidate and present the information in a more compact form. In the pursuit of high performance lithium-ion batteries, a deep understanding of the mechanisms surrounding the degradation is vital. This paper highlights the five primary causes of degradation, namely the growth of the SEI layer, lithium plating, cathode metal dissolution, and particle cracking & fracturing. These processes are all interconnected with three main underlying modes of degradation: loss of lithium inventory, loss of active material, and impedance increase. From the user's perspective, all these degradation modes result in two main noticeable effects: capacity fade and power fade.

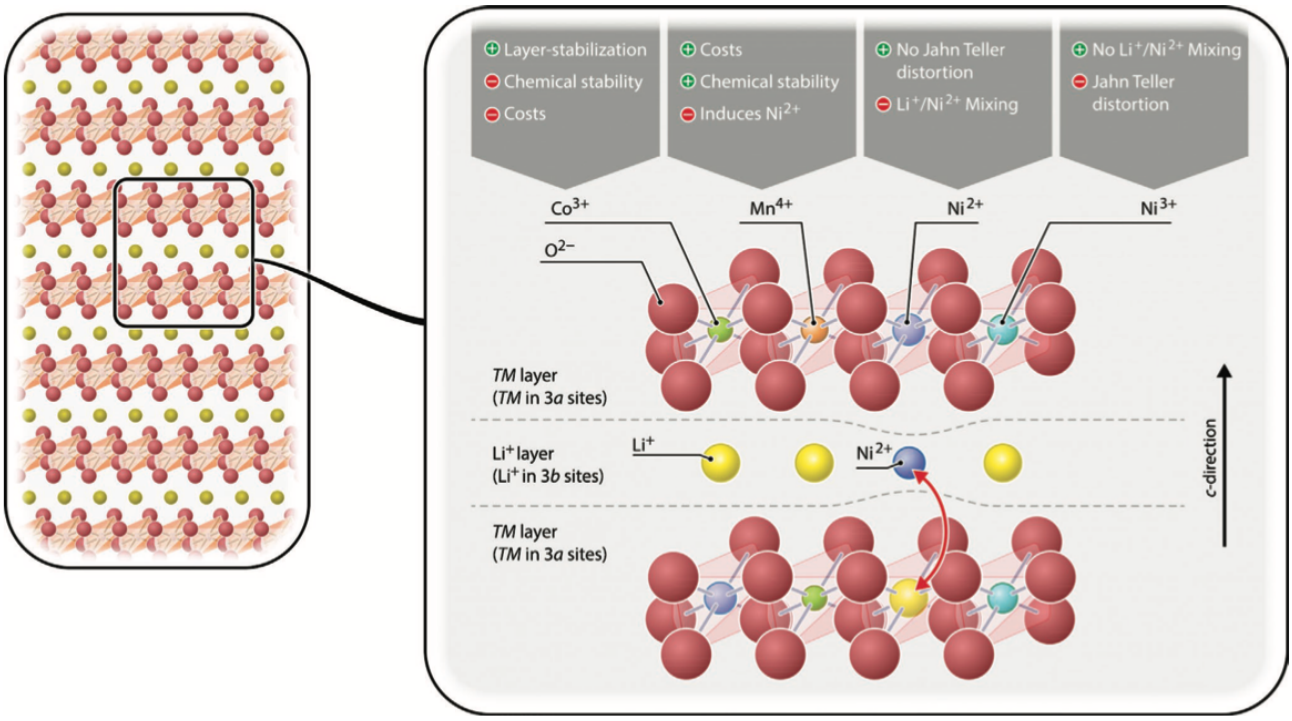

Fig. 22: Showing the crystal structure of NMC based cathode at the advantaged and disadvantage of each transition metal in the structure. that is, layered oxides like NCM.[96] [91].

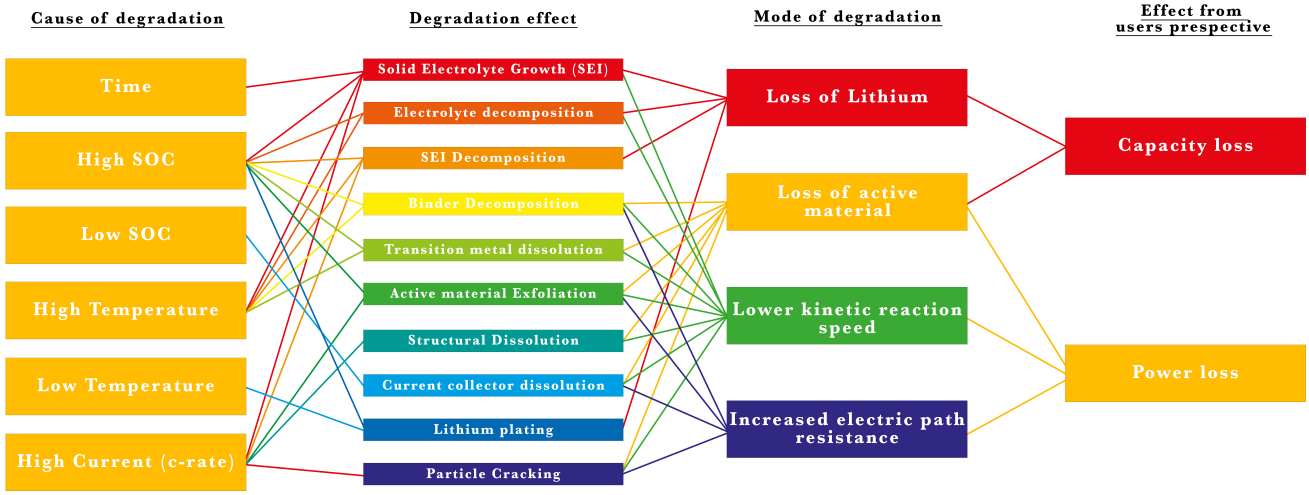

Fig. 23: The complex interaction between the underlying degradation processes and their interplay in contribution to each other *recreated by inspiration from* [3].

These effects can only partially be controlled by the user, having only influence on three external factors that impact degradation: temperature, State Of Charge (SOC), and charge/discharge profile.

Degradation does not follow a singular path towards the end of a cell's life; multiple paths can be identified that lead to its end of use. The interconnected nature of the processes occurring inside the cell makes explaining and predicting the non-linear degradation knee-point a complex endeavor. One possible path that can be taken to explain this behavior is the growth of the SEI layer, which leads to increased anode over-potential, thereby opening up the possibility of lithium plating and further SEI growth. Some research suggests that the onset of lithium plating is linked to the non-linear knee-point of the degradation trend. Another path would be that the growing SEI layer consumes electrolyte, reducing the ionic transfer conductivity, which can become the primary bottleneck and cause non-linear degradation if the conductivity falls below a certain threshold, ultimately leading to cell drying. Or that the metal dissolution and mixing of the transition metals of the cathode crystal structure caused by acid attack releases oxygen and SEI growth and thus capacity and power fade.

The precise path that leads to the end of a cell's life is likely a combination of all the mentioned degradation processes, which are determined by the overall usage of the cell and its chemistry.

It is worth noting that the majority of degradation research focuses on the anode side of the cell, which is the electrode most affected by capacity and power fade due to the ever lasting growth of the SEI layer. However, the effects of the cathode on SEI formation on the anode must also be taken into account, particularly with the industry trend of higher nickel-based NMC cells that are prone to metal dissolution.
The final aspect that needs to be noted is the potential of optimizing the electrolyte and its solvents to increase cell performance and slow down degradation mechanisms. Electrolyte additives and electrode coatings are promising methods that can be the next logical step to improve the cell's capabilities.

This paper aims to condense the interesting and significant research being conducted in the field of exploring degradation processes inside lithium-ion batteries into a comprehensive document.